

PyRTlib: an educational Python-based library for non-scattering atmospheric microwave radiative transfer computations

Salvatore Larosa¹, Domenico Cimini^{1,2}, Donatello Gallucci¹, Saverio Teodosio Nilo¹, and Filomena Romano¹

5 ¹National Research Council of Italy, Institute of Methodologies for Environmental Analysis (CNR-IMAA), Tito Scalo (Potenza), 85050, Italy

²CETEMPS, University of L'Aquila, L'Aquila, 67100, Italy

Correspondence to: Salvatore Larosa (salvatore-larosa@cnr.it)

Abstract. This article introduces PyRTlib, a new standalone Python package for non-scattering line-by-line microwave Radiative Transfer simulations. PyRTlib is a flexible and user-friendly tool for computing down and up-welling brightness temperatures and related quantities (e.g., atmospheric absorption, optical depth, opacity, mean radiating temperature) written in Python, a language commonly used nowadays for scientific software development especially by students and early career scientists. PyRTlib allows simulating observations from ground-based, airborne, and satellite microwave sensors in clear sky and in cloudy conditions (under non-scattering Rayleigh approximation). The intention for PyRTlib is not to be a competitor for state-of-the-art atmospheric radiative transfer codes that excel for speed and/or versatility (e.g., ARTS, RTTOV). The intention is to provide an educational tool, completely written in Python, to readily simulate atmospheric microwave radiative transfer from a variety of input profiles, including predefined climatologies, global radiosonde archives, and model reanalysis. The paper presents quick examples for the built in modules to access popular open data archives. The paper also presents examples for computing simulated brightness temperature for different platforms (ground-based, airborne, and satellite), using various input profiles, showing how to easily modify other relevant parameters, such as observing angle (zenith, nadir, slant), surface emissivity, and gas absorption model. PyRTlib can be easily embedded in other Python codes needing atmospheric microwave radiative transfer (e.g., surface emissivity models and retrievals). Despite its simplicity, PyRTlib can be readily used to produce present-day scientific results, as demonstrated by two examples showing (*i*) absorption model comparison and validation with ground-based radiometric observations and (*ii*) uncertainty propagation of spectroscopic parameters through the radiative transfer calculations following a rigorous approach. To our knowledge, the uncertainty estimate is not provided by any other currently available microwave radiative transfer code, making PyRTlib unique for this aspect in the atmospheric microwave radiative transfer code scenario.

1 Introduction

30 Radiative transfer (RT) models play a fundamental role in atmospheric sciences, as they are broadly used to simulate how electromagnetic radiation travels through the atmosphere as it interacts with atmospheric constituents (such as gases, aerosols and hydrometeors) through absorption, emission, scattering, and refraction. RT models are commonly used as forward operators to simulate and understand remote sensing observations from any platform, ground-based, airborne or spaceborne. RT calculations depend on the state of the atmosphere (pressure, temperature, composition), the optical properties of the atmospheric constituents (molecules and particles), the simulated observing geometry, and the spectral range. Given a set of specifications on spectral range, atmospheric conditions, and observing geometry, the RT model is able to compute the atmospheric opacity and the observations simulated accordingly. Simulated observations are then used in a broad range of applications, from atmospheric process understanding, the retrieval of atmospheric variables, to data assimilation into Numerical Weather Prediction (NWP) models. Although the theoretical aspects of wave-atmosphere interactions are essentially the same throughout the electromagnetic spectrum, different RT models have been developed to account for the specific features of limited spectral ranges, such as the visible, infrared, and microwave portions of the electromagnetic spectrum. In particular, several microwave (MW) RT models have been developed throughout the years to serve the needs of passive remote sensing from MW radiometers (e.g., Liebe, 1989; Buehler et al., 2005; Rosenkranz, 2017). Many examples are available in the open literature on the use of MW RT models for atmospheric sciences, including but not limited to: process understanding (Tripoli et al., 2005; Martinet et al 2017), atmospheric retrieval development (Eriksson et al., 2005; Boukabara et al., 2013; Sanò et al., 2015; Larosa et al., 2023), MW instrument design and validation (Buehler et al., 2012; Fox et al., 2017), data assimilation into NWP model (Eyre et al., 2020; Martinet et al., 2020), instrument synergy (Marzano et al., 1999; Turner and Löhnert, 2021; Cimini et al., 2023). A variety of software codes has been developed throughout the past three decades for implementing different flavours of available MW RT models, differing for features, assumptions, approximations, as well as coding languages. Among the different features, RT codes may be classified in scattering or non-scattering (i.e., considering absorption only). Similarly, RT codes may be classified as line-by-line, meaning that RT can be modelled at any frequency from the contributions of many gas absorption lines, or parameterized, meaning that RT can be modelled at a limited number of channels for which the optical depth is parameterized considering their spectral response function, initially trained with line-by-line calculations. Other assumptions include the observing geometry, going from plane-parallel one dimensional (1-D) calculations that consider the atmosphere state changing only in the vertical dimension, to higher dimensional (2-D or 3-D) geometries, which allows consideration of the horizontal spatial inhomogeneity, to spherical geometry, allowing to properly model the atmospheric shape and its effect on the bending angle of the radiation path. Although RT codes enabling line-by-line, scattering, and spherical geometry computations are much more complex and computational demanding than the parametrized, non-scattering, and 1-D plane-parallel assumptions, they allow more accurate modelling of the impact of spectral resolution, particle size, and 3-D distribution, respectively. Concerning the coding language, most of MW RT software codes are available in compiled programming languages such as C, C++ and Fortran. However, the interpreted programming

language Python has become increasingly popular for scientific computing in the last decades, thanks to its numerous extension packages, and it is now widely considered the language of choice in many areas, including atmospheric science. Therefore, some of the available RT codes allow users to access their features by running Python modules as wrapper of the core software, although the core software needs to be compiled from source or in binary form to access such modules. There are also cases for which the original code has been translated into Python. Table 1.1 reports a list of most popular MW RT codes, by no means complete, with their key features and access information. In the following, a brief introduction is given of the most relevant MW RT codes for this paper.

Table 1.1: List of popular codes suitable for atmospheric radiative transfer in the microwave spectral region.

Name	References	line-by-line/band	Scattering	Language	License	Access
ARTS	Eriksson et al., 2011; Buehler et al., 2018	line-by-line	Yes	C++ (python interface as wrapper)	GPL v3	https://www.radiativetransfer.org/
CRTM	Han et al., 2006; Ding et al., 2011; Wei et al., 2022	line-by-line/band	Yes	Fortran (python interface as wrapper)	CC0 v1.0	https://www.jcsda.org/jcsda-project-community-radiative-transfer-model
MonoRTM	Clough et al., 2005	line-by-line	Yes	Fortran	GPL	http://rtweb.aer.com/monortm_frame.html
PAMTRA	Mech et al., 2020	line-by-line	Yes	Fortran (python interface as wrapper)	GPL v3	https://pamtra.readthedocs.io/
Py4CATS	Schreier et al., 2019	line-by-line	No	Python	GPL	https://atmos.eoc.dlr.de/tools/Py4CATS/
RTTOV	Saunders et al., 2018	band	Yes	Fortran (python interface as wrapper)	available on request	https://nwp-saf.eumetsat.int/site/software/rttov/
RTTOV-gb	De Angelis et al., 2016 Cimini et al., 2019	line-by-line and band	Yes	Fortran	available on request	https://nwp-saf.eumetsat.int/site/software/rttov-gb/
TBUPDN	Rosenkranz, 2017	line-by-line and band	No	Fortran	freely available	http://cetemps.aquila.infn.it/rttovgb/lblmrt_ns.html

ARTS: The Atmospheric Radiative Transfer Simulator (ARTS) is a radiative transfer model suitable for calculations from the microwave to the thermal infrared spectral range (Buehler et al., 2005; Eriksson et al., 2011; Buehler et al., 2018). ARTS is

implemented in C++ with a modular design, allowing the flexibility for performing many different applications concerning radiative transfer calculations in all viewing geometries from inside or outside the atmosphere: uplooking, downlooking, limb-
75 looking. ARTS allows the choice of different state of the art absorption models, including line-by-line from HITRAN or other catalogues plus various absorption continuum parameterizations. It is fully polarized, allowing RT calculations from 1 to 4 Stokes components. It allows scattering computations from spherical and non-spherical atmospheric particles. It also provides analytical or semi-analytical Jacobians for a large set of state parameters. It supports XML and NetCDF file format for data
80 import and export. ARTS can be run standalone or through external tools, such as PyARTS, a Python package that serves as wrapper for the main ARTS core library. PyARTS is part of the ARTS source repository. PyARTS provides an interactive interface to the ARTS engine for running radiative transfer simulations and has many ARTS built-in types for the manipulation of input data and the evaluation simulation results. However, PyARTS cannot be run as a standalone python package as it needs ARTS built before.

85

CRTM: The Community Radiative Transfer Model (CRTM; Han et al., 2006; Ding et al., 2011; Wei et al., 2022) is a fast radiative transfer model developed to efficiently simulate specific spaceborne Earth observing sensors. The CRTM was developed by the U.S. Joint Center for Satellite Data Assimilation (JCSDA) to be a library for users to link to from other models. However, CRTM can be run in "stand-alone" mode. CRTM is a sensor-based RT model, supporting more than 100
90 sensors on meteorological and other remote sensing satellites, covering wavelengths ranging from the visible through the microwave. The source code is written in standard Fortran95 and makes extensive use of modules and derived type data structures. CRTM includes both the forward model and its Jacobian with respect to the input atmospheric state variables, accounting for the absorption of atmospheric gases as well as the multiple scattering of water and ice clouds composed of spherical and a variety of nonspherical particles, working under all atmospheric and surface conditions. CRTM is extensively
95 used in several applications, such as the NOAA Microwave Integrated Retrieval System (MiRS), the NCEP data assimilation system, and the NOAA STAR Integrated Calibration/Validation System Long-Term Monitoring System. CRTM can be called from Python scripts using pyCRTM, which embeds CRTM Fortran data structures and procedures directly into Python, taking advantage of both the simplicity and ease of use of Python syntax and the flexibility that comes from the extensive Python ecosystem (Karpowicz et al., 2022).

100

MonoRTM: MonoRTM represents an atmospheric radiative transfer model widely used in the scientific community to generate simulated spectral radiance ranging from the ultraviolet to the microwave region (Clough et al, 2005). It has been produced by the Atmospheric & Environmental Research (AER) and is based on the same physical properties and continuum absorption model as the Line-By-Line Radiative Transfer Model (LBLRTM), which is also developed and maintained by AER.
105 These are both Fortran 90 codes, however MonoRTM is particularly suitable to simulate a single or a set of few monochromatic wavelengths. Atmospheric molecular absorption covers all spectral regions, with molecular optical depths computed within the Monochromatic Optical Depth Model module; however, spectral radiance calculation in the presence of cloud liquid water

is only possible in the microwave range and relies on the model developed by Liebe et al. (1991). MonoRTM also accounts for molecular absorption within the spectral line center, by using the MT_CKD continuum (Clough et al., 2005). Line coupling effects, which are crucial for e.g., oxygen lines in the microwave region, are also dealt with in the code (Rosenkranz, 1988; Tretyakov et al., 2005; Cadeddu et al., 2007).

PAMTRA: This is an atmospheric radiative transfer code, namely the Passive and Active Microwave radiative TRANSfer (PAMTRA, Mech et al., 2020), specifically designed to simulate both passive microwave radiances as well as active remote sensing measurements in the presence of cloudy atmosphere. PAMTRA exploits the passive forward model to compute both upward and downward looking polarized brightness temperatures and radiances for the passive part. The active part can simulate the full radar Doppler spectrum and its higher moments (mean Doppler velocity, skewness, kurtosis). The model is built within a Fortran-Python environment, allowing the flexibility to different input/output formats and instrument characteristics (e.g., observations from ground-based, airborne or spaceborne platforms, viewing angles, etc.), with the assumption of a plane-parallel, one-dimensional homogeneous atmosphere over the horizontal direction. The user can select several operational modes among scattering and absorption models, within a wide range variety of spectroscopic parameters and databases.; the absorption model by Rosenkranz (2015) is selected as default. Alternatively, the Millimeter-wave Propagation Model (MPM93) developed by Liebe et al. (1993) can be used to simulate the atmospheric absorption by the gaseous atmosphere, considering later modifications (e.g., Turner et al., 2009; Rosenkranz, 2015). Moreover, PAMTRA implements the self-similar Rayleigh–Gans approximation (SSRGA) for both active and passive applications (Hogan et al., 2017). Generally, pyPAMTRA is used in the scientific community, which features a Python wrapper built around the Fortran core, allowing direct access from Python, without using the I/O Fortran routines. The pyPAMTRA interface makes the model user-friendly, simplifying the importing of model data, the output in terms of files or plots, and the parallel running of the code on a multicore processor or cluster machines.

Py4CAAtS: Python scripts for Computational Atmospheric Spectroscopy (Py4CAAtS, Schreier et al., 2019), is a software designed for computing atmospheric spectroscopy both in the infrared and microwave spectral regions. It was initially conceived to enable Python access to a previous Fortran 90 Generic Atmospheric Radiation Line-by-line Code (GARLIC, Schreier et al., 2014). Later on, it has become a complete self-consistent independent software, based entirely on Python numerical array processing modules, providing line by line radiances, as well as absorption cross sections and coefficients, optical depths, transmissions and weighting functions. Py4CAAtS consists of a set of modules and functions allowing to generate line-by-line cross sections for given pressure(s) and temperature(s), to combine cross sections into absorption coefficients and optical depths, and to integrate along the line-of-sight into transmission and radiance/intensity. Py4CAAtS is also user-friendly, since it offers an interactive environment and the possibility to perform batch line-by-line modeling. The software can be started within the console terminal, the Python interpreter or the Jupyter Notebook; besides, all intermediate variables can be visualized too. Py4CAAtS relies on a plane-parallel atmosphere assumption, and considers non-scattering

interactions, with the Schwarzschild equation featuring thermal emission as source only; furthermore, neither continuum nor collision-induced absorptions are taken into account as contributions to the molecular absorption, which is therefore limited to the Voigt Line shape. More recent version of Py4CATS incorporates continuum-induced absorption, simple single scattering, and modelling of aerosol optical depth, speed-dependence of pressure broadening, including line-mixing (Schreier, 2017; Schreier and Hochstaffl, 2021).

RTTOV: Similar to CRTM, the Radiative Transfer for TOVS (RTTOV) is a fast radiative transfer model for modelling passive visible, infrared and microwave downward-viewing satellite radiometers, spectrometers and interferometers (Saunders et al., 2018; Hocking et al., 2021). RTTOV is a FORTRAN 90 code designed to be incorporated within user applications for simulating satellite radiances. RTTOV is developed and maintained by the NWP Satellite Application Facility of EUMETSAT, and it is probably the most used RT code for satellite data assimilation into NWP models. Given an atmospheric profile of temperature, water vapour and, optionally, trace gases, aerosols and hydrometeors, together with surface parameters and a viewing geometry, RTTOV computes the top of atmosphere radiances for a set of space-borne sensors from past, current, and future satellite Earth observing missions. The core of RTTOV is a fast parameterisation of layer optical depths due to gas and liquid water absorption. Profiles of layer-to-space transmittances computed by the line-by-line code AMSUTRAN (Turner et al., 2019) are the basis for the training of the fast parameterisation in the microwave region. RTTOV consists in both the forward model, which simulates the upwelling radiances for a given sensor, and its Jacobian, which calculates the radiance derivatives with respect to the input atmospheric state variables. RTTOV includes scattering calculations for simulating cloudy and aerosol-affected radiances in the infrared. Scattering at MW frequencies from hydrometeors of different phases and shapes is available through the wrapper code RTTOV-SCAT (Bauer et al., 2010; Geer et al., 2021). RTTOV has a built-in graphic user interface (GUI) which allows the user to modify an atmospheric/surface profile, run RTTOV for a given instrument, produce radiances and brightness temperatures, calculate Jacobians, perform a basic retrieval, and display instantaneously the results. RTTOV is natively in Fortran, but Python wrappers are available to allow the functionality of RTTOV in Python. These wrappers provide Python bindings for the RTTOV Fortran code, making it easier for Python users to use. A ground-based version of RTTOV for simulating ground-based MW sensors is also available, though limited to version 11 (De Angelis et al., 2016; Cimini et al., 2019).

TBUPDN: The upward-downward T_b (TBUPDN) code is a library of Fortran routines for the non-scattering line-by-line microwave RT simulations (Rosenkranz, 2017). The code is developed and maintained by Philip W. Rosenkranz since more than 30 years (Rosenkranz, 1993). TBUPDN is intended as an educational tool with limited ranges of applicability, i.e. calculations of upward- and downward-propagating T_b respectively at the top and bottom of the atmosphere. The main routines can be run stand-alone or read as examples for using the subroutines (e.g., the absorption model routines) in other software programs. A major feature of TBUPDN is the continuous update of absorption routines, originally based on the MPM code, with subsequent spectroscopic modifications from most recent findings from laboratory and field campaign experiments

(Rosenkranz, 1988; 1998; 2001; 2005; Rosenkranz and Cimini, 2019; Gallucci et al., 2023). User interfaces are provided for handling I/O text files and produce encapsulated postscript figures.

180 Table 1 and the list above are meant to provide an overview of open access codes that are used extensively by the MW community, but do not pretend to be complete. Other codes suitable for atmospheric RT in the MW are available, either openly or commercially, e.g., BTRAM (Chapman et al., 2010), MODTRAN (Berk et al., 2014). Other RT codes that are available in Python or with a Python interface, although not concerning MW in Earth's atmosphere, include the following: PYDOME (Efremenko et al. 2019) for simulating satellite measurements of reflected and scattered solar radiation in the ultraviolet and visible spectral ranges; Py6S (Wilson, 2013), a Python interface to the 6S RTM (Vermote et al., 1997) designed to simulate solar radiation through atmospheres on Earth and other planets; PySMARTS module (Ayala Pelaez and Deline, 2020) contains 185 functions for calling SMARTS: Simple Model of the Atmospheric Radiative Transfer of Sunshine to compute clear sky spectral irradiances (on a tilted or horizontal receiver plane) for specified atmospheric conditions; petitRADTRANS (Mollière et al., 2019) and PYRATE (Tritsis et al., 2018) for simulating RT through atmospheres on exoplanets.

190 This paper introduces PyRTLlib, a new standalone Python package for non-scattering line-by-line microwave RT simulations. Given the premises above, one may ask: is a new RT code really needed? The intention for PyRTLlib is not to be considered a competitor for the codes mentioned above, which represent the cutting edge with their own peculiarities, in terms of efficiency, flexibility, modularity, and applicability. Nevertheless, the reasons behind the development of PyRTLlib are the following:

- 1) Develop an educational tool, similarly to TBUPDN, but in Python, which represents nowadays the most used language 195 for scientific software development, especially by students and younger scientists;
- 2) Provide user-friendly Python interfaces, similarly to PyARTS or pyPAMTRA, to compute MW RT simulations using popular datasets as input, such as radiosonde repository or global reanalysis;
- 3) Allow easy comparison of MW calculations using different atmospheric absorption models, e.g., those proposed throughout the last three decades, for any platform (ground-based, airborne, and spaceborne) and observing geometry (zenith, nadir, slant), except for limb sounding geometry (not currently implemented in PyRTLlib); 200
- 4) Provide T_B calculations with the associated uncertainty due to the uncertainty on spectroscopic parameters, following a general rigorous approach recently outlined (Cimini et al., 2018; Gallucci et al., 2023).

205 In particular, to our knowledge the uncertainty estimate is not available by any other MW RT code, making PyRTLlib unique for this aspect in the MW RT scenario. Thus, this paper provides a description of PyRTLlib version 1.0 and advocates its use through a range of examples demonstrating its value in producing passive MW simulations from notable input datasets (radiosondes, reanalysis) and for ground-based, airborne, and satellite perspectives.

The paper is structured as follows: brief introduction of the basics of equations of radiative transfer model, the main absorption model available and how profiles can be interpolated and extrapolated are discussed in section 2. The tools for retrieving and

210 managing input data from open access repositories (e.g., radiosonde observations and model reanalysis) are discussed in Section 3. Usage of the code as well as some implementation details and a few examples of applications are presented in Section 4. Section 5 summarises the conclusions and future developments, while Section 6 provides instructions for code availability and usage.

2 Radiative transfer model

215 An atmospheric RT model simulates the propagation of electromagnetic radiation through the atmosphere as it interacts with the atmospheric constituents (gases, aerosols and hydrometers) through absorption, emission, scattering, and refraction. The intensity of radiation I , also called radiance, expresses the power carried by the electromagnetic radiation along the direction of propagation per unit area and solid angle at a given frequency f . Considering an ideal blackbody radiator in local thermodynamic equilibrium at physical temperature T , the intensity of radiation I is given by the Planck function:

220

$$B_f(T) = \left(\frac{2hf^3}{c^2}\right) \left(\frac{1}{e^{\frac{hf}{kT}} - 1}\right) \quad (1)$$

where h and k are the Planck and Boltzmann constants, respectively, and c is the speed of light. From Eq. (1) comes directly the definition of brightness temperature T_B , as the temperature that a blackbody radiator should have to emit the radiance I , i.e., $I = B_f(T_B)$.

225

The relevance of radiation scattering by atmospheric particles depends on the ratio between the size of the scattering particle r and the radiation wavelength λ , so called size ratio $x = 2\pi r/\lambda = 2\pi r f/c$ (Petty, 2006). If $x \ll 1$, then the contribution of scattering can be considered negligible. That is the case at microwave and millimeter-wave frequencies ($\lesssim 1$ THz) in clear sky (no clouds). For relatively small hydrometeors (i.e., liquid and ice clouds) the size ratio is still $x < 1$, and the Rayleigh approximation is valid, for which absorption is still dominant with respect to scattering. Thus, a simplifying common assumption at microwave frequencies is to neglect atmospheric scattering, which is commonly assumed valid in absence of large particles (i.e., liquid and solid precipitation). In such a case, the Swartzchild equation applies, i.e.:

230

$$B_f(T_B) = B_f(T_{BG})e^{-\tau_f(0,\infty)} + \int_0^\infty B_f(T(s))\alpha_f(s)e^{-\tau_f(0,s)} ds \quad (2)$$

235

where s indicates the distance from the observations point along the line-of-sight, α_f indicates the atmospheric absorption coefficient, τ_f indicates the atmospheric opacity ($\tau_f(a,b) = \int_a^b \alpha_f(s)ds$), and the two extremes of the integral indicate the position where the T_B measurement is taken (0) and the position of a uniform background (∞) of temperature T_{BG} . The first term of Eq.(2) changes depending on the observing geometry. For an uplooking radiometer measuring downwelling radiation,

240 without discrete sources (such as the Sun or Moon) within the antenna field of view, $B_f(T_{BG})$ is simply equal to $B_f(T_{CBG})$, where $T_{CBG} \simeq 2.7 K$ is the microwave cosmic background brightness temperature (Rosenkranz, 1993). For a downlooking radiometer measuring upwelling radiation, e.g. from a satellite platform, a typical background is the Earth's surface, the spectral emissivity (ε_f) of which must be taken into account to model the complementary contribution of Earth's surface emission and reflection of downwelling radiation. Thus, indicating with SRF the position of the Earth's surface and TOA the top of atmosphere, $B_f(T_{BG})$ in Eq. (2) becomes:

$$B_f(T_{BG}) = (1 - \varepsilon_f) \left[B_f(T_{CBG}) e^{-\tau_f(SRF, TOA)} + \int_{SRF}^{TOA} B_f(T(s)) \alpha_f(s) e^{-\tau_f(SRF, s)} ds \right] + \varepsilon_f B_f(T_{SRF}) \quad (3)$$

The integral in the atmospheric terms in Eq. (2) and (3) is divided into the sum of integrals over each of the NL-1 layers in between the NL levels in which the atmosphere is discretized (Schroeder and Westwater, 1991). In case of uplooking simulations of downwelling radiation:

$$\int_0^\infty B_f(T(s)) \alpha_f(s) e^{-\tau_f(0, s)} ds \cong \sum_{i=2}^{NL} \int_{s_{i-1}}^{s_i} B_f(T(s)) \alpha_f(s) e^{-\tau_f(0, s)} ds \quad (4)$$

255 The integrals in the second term can be simplified by introducing a mean radiating temperature of a layer T_{MR} , such as:

$$\int_{s_{i-1}}^{s_i} B_f(T(s)) \alpha_f(s) e^{-\tau_f(0, s)} ds = B_f(T_{MR}) \int_{s_{i-1}}^{s_i} \alpha_f(s) e^{-\tau_f(0, s)} ds = B_f(T_{MR}) e^{-\tau_f(0, s_{i-1})} [1 - e^{-\tau_f(s_{i-1}, s_i)}] \quad (5)$$

where $B_f(T_{MR})$ for the layer of atmosphere between a and b is defined as:

$$B_f(T_{MR}) = \frac{\int_a^b B_f(T(s)) \alpha_f(s) e^{-\tau_f(0, s)} ds}{e^{-\tau_f(0, a)} [1 - e^{-\tau_f(a, b)}]} \quad (6)$$

$B_f(T_{MR})$ can be approximated as the weighted average of $B_f(T(s))$ from the two profile levels that form the layer:

$$B_f(T_{MR}) \simeq \frac{B_f(T(s_{i-1})) + B_f(T(s_i)) e^{-\tau_f(s_{i-1}, s_i)}}{1 + e^{-\tau_f(s_{i-1}, s_i)}} \quad (7)$$

where the exponential weight $e^{-\tau_f(s_{i-1}, s_i)}$ represents the attenuation of $B_f(T(s_i))$ over the layer between levels i and $i-1$. Note that introducing the layer transmittance $\mathbb{T} = e^{-\tau_f(s_{i-1}, s_i)}$ in Eq.(7), it becomes

$$B_f(T_{MR}) \simeq \frac{B_f(T(s_{i-1})) + B_f(T(s_i))\mathbb{T}}{1 + \mathbb{T}} \quad (8)$$

Thus, $B_f(T_{MR})$ is the average brightness temperatures at the layer boundaries, weighted by the layer transmittance, going from $B_f(T(s_{i-1}))$ to $\frac{B_f(T(s_{i-1})) + B_f(T(s_i))}{2}$ as the layer gets from totally opaque ($\mathbb{T} = 0$) to totally transparent ($\mathbb{T} = 1$). Other weighting options, such as the so-called linear-in-tau, are used elsewhere (Saunders et al., 2018). The contribution of each layer is then summed up as in Eq. (4) (Schroeder and Westwater, 1991). The case of downlooking observations can be simply derived from the above.

2.1 Modelling atmospheric absorption

Modelling atmospheric absorption is a crucial component of RT codes. Absorption models are based on parameterized equations to calculate atmospheric absorption (α_f in Eq. (2)) given the constituents' concentration and their thermodynamic conditions (Rosenkranz, 1993). Note that, as introduced earlier, PyRTlib is a non-scattering RT code, i.e., it assumes that attenuation is due entirely to absorption by atmospheric gases and cloud water, while it neglects the extinction due to particle scattering. Concerning atmospheric gases, PyRTlib considers the absorption contribution by nitrogen and oxygen (also called dry air contribution, α_{dry}) and water vapour (wet contribution, α_{wet}). These three species sum up to more than 99% of the atmospheric gas mixture and account for most of the gas absorption in the MW spectrum. In general, the gas absorption is expressed as the sum of a resonant component (due to absorption lines of individual molecules) and a non-resonant component (due to the interaction between molecules): $\alpha_{total} = \alpha_{res} + \alpha_{nr}$. The resonant absorption is modeled computing the contribution of each significant absorption line (line-by-line), so that for a specified molecular species with n molecules per unit volume the power absorption coefficient at frequency ν is given by:

$$\alpha_{res} = \sum_i \alpha_{line}(\nu, \nu_i) = n \sum_i S_i(T) F(\nu, \nu_i) \quad (9)$$

where, calling k the Boltzmann's constant and E_{low} the energy of the lower level

$$S_i(T) = S_i(T_0) \theta^{n_s} \exp\left(\frac{E_{low} + h\nu_i/2}{kT_0} (1 - \theta)\right) \quad (10)$$

is the line intensity at temperature T , which, with respect to its value at the reference temperature T_0 , depends on the so-called inverse temperature $\theta = \frac{T_0}{T}$ and the temperature exponent n_s , and

$$300 \quad F(\nu, \nu_i) = \frac{1}{\pi} \left(\frac{\nu}{\nu_i} \right)^2 \left[\frac{\Delta\nu_i + Y_i \cdot (\nu - \nu_i)}{\Delta\nu_i^2 + (\nu - \nu_i)^2} + \frac{\Delta\nu_i - Y_i \cdot (\nu + \nu_i)}{\Delta\nu_i^2 + (\nu + \nu_i)^2} \right] \quad (11)$$

is the line-shape function of the i^{th} absorption line at center frequency ν_i , with half-width at half amplitude $\Delta\nu_i$, and mixing parameter Y_i , which all have some dependence on temperature and/or pressure (Rosenkranz, 1993; Cimini et al., 2018). Conversely, the non-resonant absorption is characterized by smooth frequency dependence. The dry-air contribution is modelled through a frequency-dependent factor $f(\nu)$ to fit experimental data as $\alpha_{nr_dry}(\nu, T) = C_d f(\nu) \theta^{n_d} P_d^2 \nu^2$, where C_d is the intensity coefficient, n_d the relative temperature-dependence exponent, and P_d the partial pressures of dry air. Similarly, the water vapor non-resonant absorption is modelled through the contribution of two terms corresponding to the interaction of water molecules with each other (self component), and between water molecules and air molecules (foreign component): $\alpha_{nr_wv}(\nu, T) = (C_s \theta^{n_{cs}+3} P_w^2 + C_f \theta^{n_{cf}+3} P_d P_w) \cdot \nu^2$ where P_w is the partial pressures of water vapor, while C_s and C_f are empirical intensity coefficients respectively for self- and foreign-induced absorption with their respective temperature-dependence exponents (n_{cs}, n_{cf}). PyRtlib also offers the option to add the contribution of ozone (α_{O_3}); this causes a relatively small absorption increase in very narrow spectral ranges due to many nearly monochromatic spectral lines at the expense of slower computations. Concerning hydrometeors, the absorption of cloud liquid (α_{liq}) and ice (α_{ice}) particles are considered, assuming the Rayleigh absorption approximation of Mie's forward scattering theory. This allows to express the cloud absorption as a simple function of the complex dielectric constant of liquid (ϵ_{liq}) and ice (ϵ_{ice}) water, e.g.:

$$\alpha_{liq} = C_{liq} L \nu \Im((\epsilon_{liq} - 1)/(\epsilon_{liq} + 2)) \quad (12)$$

$$\alpha_{ice} = C_{ice} I \nu \Im((\epsilon_{ice} - 1)/(\epsilon_{ice} + 2)) \quad (13)$$

320 where \Im indicates the imaginary part, C_{liq} and C_{ice} are constants, while L and I are respectively the liquid and ice water mass content per unit of air volume. Note that $\alpha_{dry}, \alpha_{wet}, \alpha_{O_3}, \alpha_{liq}$, and α_{ice} all depend on frequency and location in space, although not shown for simplicity. In fact, the sum $\alpha_{dry} + \alpha_{wet} + \alpha_{O_3} + \alpha_{liq} + \alpha_{ice}$ represents $\alpha_f(s)$ in Equations (2) and (3). Of course, the terms α_{liq} and α_{ice} are zero in clear sky conditions while α_{O_3} is zero if ozone contribution is neglected. Absorption models for computing $\alpha_{dry}, \alpha_{wet}, \alpha_{O_3}, \alpha_{liq}$, and α_{ice} from the constituents' concentration and the thermodynamic conditions are available in the open literature (e.g., Rosenkranz, 1993). These models rely on parameterized equations and spectroscopic parameters, valid up to 1 THz, determined through theoretical calculations and/or laboratory and field measurements. These settings are continuously updated and improved (Liebe et al., 1989; Rosenkranz, 1998; Liljegren et al., 2005; Turner et al., 2009; Mlawer et al., 2012; Koshelev et al., 2018). The proposed changes are occasionally summarised in review articles (e.g., Rothman et al., 2005; Gordon et al., 2017, Rosenkranz, 1998; 2017; Tretyakov, 2016). In particular, PyRtlib implements absorption routines originally based on the MPM code (Liebe, 1989), with subsequent spectroscopic modifications from laboratory and field campaign experiments (Rosenkranz, 1988; 1998; 2005; 2015; 2017; Rosenkranz and Cimini, 2019;

Koshelev et al., 2021; 2022). These changes have been summarised in two papers (Cimini et al., 2018; Gallucci et al., 2023). PyRTlib provides the possibility to easily compare different absorption model configurations, as discussed in one of the examples in Section 4. In case the input profile contains non-zero cloud liquid and/or ice water, the relative absorption is computed and added to the total absorption. The cloud absorption model used here assumes Rayleigh approximation, under which scattering is negligible relative to absorption, and absorption is independent of cloud particle size distribution. These assumptions restrict the model to non-precipitating clouds with particle radii less than about 100 μm for frequency less than 100 GHz. Therefore, in its current version, PyRTlib is not adequate for modelling extinction by rain or large cloud droplets or ice particles. Absorption by cloud ice (α_{ice}) particles is implemented following the algorithms described in Schroeder & Westwater (1991). More than one model are implemented for the absorption by cloud liquid (α_{liq}), i.e. the one from Liebe et al. (1991) and later improvements (i.e., Liebe et al., 1993). Another model, as in Rosenkranz (2015), is also implemented. This model was developed to be applicable up to 60°C, but it is specifically recommended for temperatures as low as -25°C for modeling the absorption of supercooled liquid water particles. Therefore, currently three models for liquid cloud absorption are available within PyRTlib and can be alternatively selected by the user.

2.2 Modelling a continuous atmosphere

To compute absorption throughout the atmosphere, the gas concentrations and thermodynamic profiles are to be provided in input. While O₂ concentration is assumed constant with altitude, concentration of H₂O (and O₃, if considered) is usually variable with altitude, and similarly for air pressure and temperature. These inputs may come from atmospheric measurements (e.g., balloon-borne radiosoundings) or atmospheric model output (e.g., NWP model), and are typically available at discrete levels. To compute realistic simulated observations from ground-based or satellite platforms, the profiles must cover the vertical range from the Earth surface to a reasonable top-of-atmosphere (TOA), where the atmosphere is so rare that it affects MW radiation negligibly. In practice, the TOA is assumed to approximate the infinite limits on the integral in Eq.(2). For simulations of downwelling radiation, the vertical range could be reduced at the bottom to the height of the simulated receiving antenna (e.g., for the simulations of airborne or elevated instruments). PyRTlib provides functions to extend the input profile to a TOA at 0.1 mb (following Schroeder and Westwater, 1991), a pressure well below the minimum pressure (i.e., maximum altitude) reached by radiosoundings. This profile extension follows a recommendation (ITU-R P.835-6, 2017) by the International Telecommunication Union - Radiocommunication Sector (ITU-R), providing expressions and data for reference standard atmospheres required for the calculation of gaseous attenuation on Earth-space paths. In particular, PyRTlib currently implements the data in Annex 1, i.e., standard atmospheres to be used to determine temperature, pressure and water-vapour pressure as a function of altitude, when more reliable local data are not available. Data in Annex 3, i.e. providing vertical profiles capturing diurnal, monthly, and seasonal variations from ECMWF 15-year data set re-analysis (ERA15) will be implemented in future PyRTlib releases. Another option is to increase the level density by adding levels through interpolation. This option allows a maximum pressure difference between a pair of adjacent profile levels. If the pressure difference in the

365 input profile exceeds the specified maximum value, PyRTLb divides the layer between the two levels into the smallest number of equally-spaced pressure levels that differ by less than the specified maximum value, using linear interpolation in natural logarithm of pressure.

2.3 Modelling observation geometry

370 The input height profile h is assumed to represent the vertical line-of-sight ray path coordinate. This corresponds to s in Eq.(2) for uplooking zenith-pointing simulations and to h_{TOA-S} for downlooking nadir-pointing simulations. For observing angles different from zenith or nadir, the ray path increases due to the slant path through the atmosphere. Considering a plane-parallel atmosphere, the increase effectively corresponds to the multiplicative factor $secant\phi$, where ϕ is angle with respect to zenith/nadir (or $cosecant\theta$, if the elevation angle θ is considered). This approximation only requires the elevation angle θ and
 375 the profile of the atmospheric thermodynamical status (pressure, temperature, relative humidity, cloud water content) as function of altitude over the Earth surface (h), and it is the default option in PyRTLb. A one-dimension spherical atmosphere can also be considered, which assumes the atmosphere as uniform concentric layers around a smooth spherical Earth. Following Schroeder and Westwater (1991), the ray path for a spherically stratified atmosphere is modelled through the Snell's law for polar coordinates:

$$380 \quad n r \cos\theta = constant \quad (14)$$

where n is the atmospheric refractive index and r is the radial distance from the center of the Earth to a point on the ray path. All these qualities depend only on height above the surface. The radiance distance r is assumed as the Earth geoid radius (R_E) plus the height above the surface. Note that the constant in Eq. (14) must be set in one point of the ray path. This is currently
 385 set at the lowest available atmospheric level, which imposes the limitation that PyRTLb version 1.0 cannot simulate limb sounding observations. The refractive index n is computed from the dry and wet refractivity (N_d and N_w , respectively) and the inverse compressibility of dry air and water vapor (Z_d^{-1} and Z_w^{-1} , respectively) through the following non-dispersive model:

$$390 \quad n = 1 + (N_d + N_w) \cdot 10^{-6} \quad (15)$$

$$N_d = k_1 \left(\frac{P_d}{T} \right) Z_d^{-1} \quad (16)$$

$$N_w = \left(k_2 \frac{e}{T} + k_3 \frac{e}{T^2} \right) Z_w^{-1} \quad (17)$$

$$Z_d^{-1} = 1 + P_d \left(57.90 \cdot 10^{-8} \left(1 + \frac{0.52}{T} \right) - 9.4611 \cdot 10^{-4} \frac{T^{-273.16}}{T^2} \right) \quad (18)$$

$$Z_w^{-1} = 1 + 1650 \frac{e}{T^3} (1 - 0.01317 T_c + 1.75 \cdot 10^{-4} T_c^2 + 1.44 \cdot 10^{-6} T_c^3) \quad (19)$$

395

where T , e , P_d are respectively the air temperature (K), water vapour partial pressure, and dry air partial pressure (hPa), while T_c is the air temperature in °C ($T_c = T - 273.16$). The three k coefficients ($k_1 = 77.604$, $k_2 = 64.79$, $k_3 = 3.776 \cdot 10^5$) are given by Saastamoinen, 1972 and references therein. PyRTlib optionally provides a slightly modified definition for computing the dry and wet refractivity terms, though leaving the total refractivity and the refractive index unaffected, which is commonly used in geodesy (ESA TN, 2019). Finally, for each specified observing angle a ray-tracing algorithm based on Eq. (14) is used to compute the refracted path length between each pair of adjacent profile levels. The integrals along the ray path are computed assuming that the integrand variable decays exponentially with height within the layer defined by a pair of adjacent levels. With this assumption, the integral along one layer of a general integrand variable X is given by (Schroeder and Westwater, 1991):

$$\int_{s_{i-1}}^i X(s) ds = (s_i - s_{i-1}) [(X(s_i) - X(s_{i-1})) / \ln(X(s_i)/X(s_{i-1}))] \quad (20)$$

This is used to compute path-integrated quantities, such as layer-integrated absorption profiles for RT calculations as well as total integrals along the entire path, such as precipitable water vapour, path delay (excess path length) due to dry air and to water vapour, and total absorption due to water vapour, dry air, and cloud liquid/ice.

3 Tools for retrieving input data

PyRTlib comes with a built-in module to easily retrieve meteorological data that can be used as input for the RT calculations. These modules allow easy access to data repositories of radiosonde observations (RAOB) and model reanalysis. The RAOB repositories currently considered in PyRTlib are the University of Wyoming Upper Air Archive (UWYO, 2015) and the U.S. National Center for Environmental Information (NCEI) Integrated Radiosonde Archive (IGRA) version 2 (Durre et al., 2016). These datasets are retrieved by using part of the Siphon (<https://github.com/Unidata/siphon>) library from UNIDATA. Concerning model reanalysis, PyRTlib currently considers the ECMWF 5th-generation Reanalysis (ERA5) as accessible from the Climate Data Store Application Program Interface (CDS API) (<https://github.com/ecmwf/cdsapi>) service. The following subsections describe how the above datasets can be accessed through PyRTlib.

3.1 Radiosondes

Balloon-borne measurements from radiosondes provide high resolution accurate profiles of temperature, humidity and wind from the altitude of the launching site up to the altitude where the balloon bursts (~ 30 km for a successful launch). This information is an important piece of the global observing system, and it is widely used in atmospheric research and related services, such as operational meteorology, air quality forecast, climatology, NWP validation and data assimilation, and finally the calibration and validation of remote sensing observations. The Wyoming Upper Air Archive from the University of Wyoming consists of radiosonde balloons from more than 628 globally distributed stations over the world. The data are

available at synoptic hours (00-06-12-18 UTC) starting from 1973. The available variables are latitude, longitude and elevation of each launching station, and the atmospheric profiles of pressure, geopotential height, temperature, dew point temperature, frost point temperature, relative humidity, relative humidity with respect to ice, water vapour mixing ratio, wind direction, wind speed, potential temperature, equivalent potential temperature, and virtual potential temperature. The vertical resolution varies from tens of meters in the lower layers to hundreds of meters near the tropopause, changing according to the site and weather conditions. Listing 1 shows the code to retrieve and plot data measured by one radiosonde launched at 12 UTC 22 April 2021 from the station named LIRE (Pratica di Mare, Italy), leading to the graphic output in Figure 1. Data from any other station available on the Wyoming Upper Air Archive can be accessed knowing the station name or number that can be found through their web interface (<https://weather.uwyo.edu/upperair/sounding.html>).

```
import matplotlib.pyplot as plt
from datetime import datetime

from pyrtlib.apiwebservices import WyomingUpperAir
from pyrtlib.utils import to_kelvin

date = datetime(2021, 4, 22, 12)
station = 'LIRE'
df = WyomingUpperAir.request_data(date, station)
df.temperature = to_kelvin(df.temperature)
df.plot("temperature", 'pressure',
        xlabel="T [K]", ylabel="P [hPa]",
        grid=True, legend=False)
df.plot("rh", 'pressure',
        xlabel="RH [%]", ylabel="P [hPa]",
        grid=True, legend=False)
plt.gca().invert_yaxis()
plt.yscale('log')
```

Listing 1. Example code using PyRTlib module to retrieve radiosonde data from the Wyoming Upper Air archive.

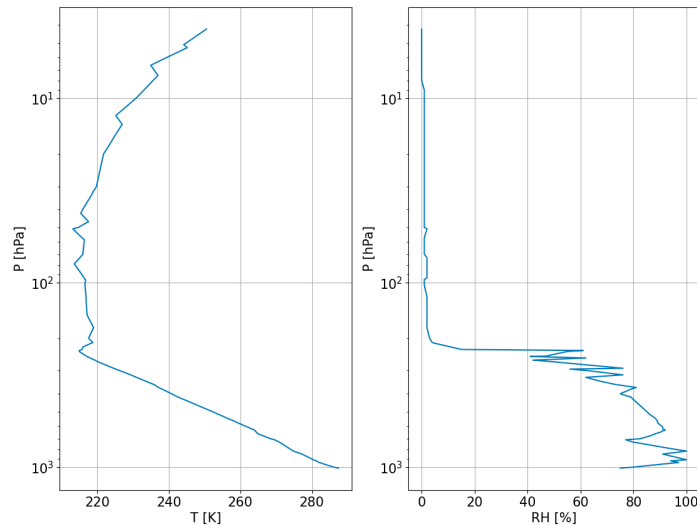


Figure 1. Graphical output of Listing 1, showing atmospheric profiles measured by the radiosonde launched at 12:00 UTC on 22 April 2021 from the LIRE station (Pratica di Mare, Italy). Left: Temperature profile (K). Right: Relative Humidity (%).

440

Another well-known repository for radiosonde data is the Integrated Global Radiosonde Archive (IGRA), consisting of radiosonde and pilot balloon observations from more than 2800 stations distributed globally. The earliest data dates back to 1905 and recent data becomes available in near real time from around 800 stations all over the world. The recording period, temporal and vertical resolution for each station vary over time. Observations are available at standard and variable pressure levels, fixed and variable height wind levels, surface and tropopause. Variables include time since launch and profiles of atmospheric pressure, temperature, geopotential height, dew point depression, wind direction and speed at a variable number of levels, including surface, tropopause, mandatory standard and optional significant levels. The data are released after a quality assurance algorithm performed by the archiving system, checking for format problems, physically implausible values, internal inconsistencies among variables, climatological outliers, and temporal and vertical inconsistencies (Durre et al., 2016; 2018).

445

The IGRA is accessible through NCEI, which also provides access to IGRA station metadata, including information about changes in the station's location, instrumentation, and observation practices over time, that may be useful for interpreting the data. Listing 2 shows the code to retrieve and plot data measured by one radiosonde launched at 12 UTC 22 June 2022 from the station network-id SPM00060018 (Tenerife, Spain), leading to the graphic output in Figure 2. Data from any other station available on IGRA can be accessed knowing the station network-id that can be found through their web interface

450

(<https://www.ncei.noaa.gov/data/integrated-global-radiosonde-archive/doc/igra2-station-list.txt>). Note that PyRTlib provides tools to convert atmospheric moisture variables to the standard input relative humidity (e.g., in the given example, the function `dewpoint2rh` computes relative humidity from dew point depression and physical temperature). PyRTlib then internally computes water vapour pressure and density from temperature and relative humidity using the Goff-Gratch formulas for saturation vapour pressure over liquid and ice water, according to a user-specified switch that determines whether the saturation vapour pressure is calculated over water throughout the profile or over ice when temperature is below a given threshold.

455

460

```
from pyrtlib.apiwebservices import IGRUpperAir
from pyrtlib.utils import to_kelvin, dewpoint2rh
from datetime import datetime

date = datetime(2022, 6, 22, 12)
station = 'SPM00060018'
df, header = IGRUpperAir.request_data(date, station)
df = df[df.pressure.notna() &
        df.temperature.notna() &
        df.dewpoint.notna() &
        df.height.notna()]

rh = dewpoint2rh(df.dewpoint, df.temperature).values
df.relative_humidity = rh * 100
df.temperature = to_kelvin(df.temperature)

df.plot("temperature", 'pressure',
        xlabel="T [K]", ylabel="P [hPa]",
```



```

        grid=True, legend=False)
df.plot("relative_humidity", 'pressure',
        xlabel="RH [%]", ylabel="P [hPa]",
        grid=True, legend=False)

plt.gca().invert_yaxis()
plt.yscale('log')

```

Listing 2. Example code using PyRTlib module to retrieve radiosonde data from the IGRA2 archive.

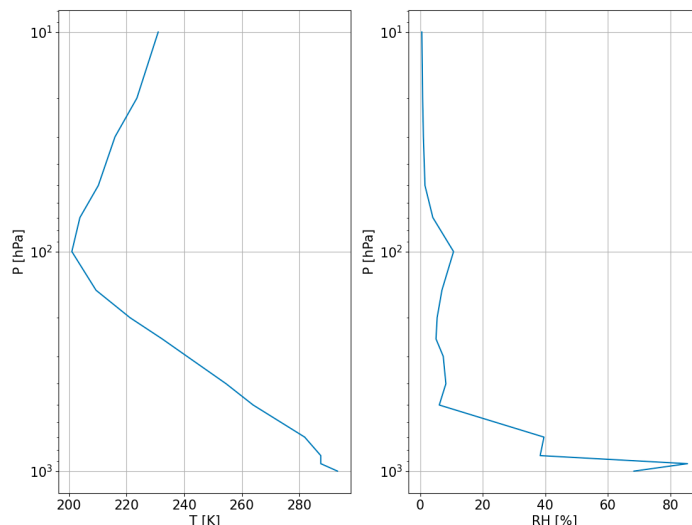


Figure 2. Graphical output of Listing 2, showing atmospheric profiles measured by the radiosonde launched at 12:00 UTC on 22 June 2022 from the station SPM00060018 (Tenerife, Spain). Left: Temperature profile (K). Right: Relative Humidity (%).

465 3.2 Model reanalysis

Model reanalysis is an optimal combination of past observations with atmospheric models to provide the most accurate representation of the status of the atmosphere at sub-daily intervals on a regular 3D spatial grid. In short, forecast models and 4D data assimilation systems are used periodically to “reanalyse” archived observations based on variational optimal estimation method. Model reanalysis has substantially evolved during recent decades in generating a consistent time series of multiple climate variables, and are nowadays among the most-used datasets in geophysical sciences. ERA5 is the fifth and latest generation of global climate reanalysis produced by ECMWF, providing hourly data of many atmospheric, land-surface and sea-state parameters together with estimates of uncertainty. ERA5 is based on the most recent and advanced version of the ECMWF Integrated Forecasting System (IFS) model and significantly improved compared to its predecessors (Hersbach et al., 2020). ERA5 is produced and continuously updated by the Copernicus Climate Change Service (C3S) and made available through the Climate Data Store (CDS). ERA5 data are archived on a reduced Gaussian grid, which has quasi-uniform spacing over the globe, at native resolution of 0.28125 degrees (31 km), from the surface up to about 80 km height. Data can be accessed in either GRIB (native) or NetCDF format. PyRTlib implements data retrieval in NetCDF format, which is automatically converted and interpolated from the native grids to a regular latitude/longitude grid (0.125° × 0.125° grid, i.e.

~16 km at the equator) at 37 pressure levels. Hourly estimates of a large number of gridded atmospheric, land and oceanic
480 climate variables are included from 1979 onwards, with a 5-day delay from real time. Among the available variables the
following are selected as input for PyRTLlib: temperature, relative humidity, specific cloud ice water content, specific cloud
liquid water content, ozone mass mixing ratio. Listing 3 shows the code to retrieve ERA5 data from the Copernicus CDS for
the nearest grid point to a location in Southern Italy (longitude 16.04°; latitude 39.44°) on 16 May 2023 at 18:00 UTC. Listing
3 also shows tools to convert the native units for cloud water variables (mass mixing ratios, kg/kg) in liquid and ice water
485 density (g/m^3), and plots cloud liquid water content (CLWC), cloud ice water content (CIWC), and ozone mass mixing ratio
(Figure 3). Data from any other location worldwide from 1979 onwards with a 5-day delay from real time can be accessed by
simply providing longitude, latitude, date and hour. Note that to access the ERA5 dataset requires configuring an API key.
Step-by-step instructions to create an API key are available at: <https://cds.climate.copernicus.eu/api-how-to>.

```
import tempfile
from pyrtlib.apiwebservices import ERA5Reanalysis
from pyrtlib.utils import kgkg_to_kgm3

lonlat = (16.04, 39.44)
date = datetime(2023, 5, 16, 18)
nc_file = ERA5Reanalysis.request_data(tempfile.gettempdir(), date, lonlat)

df_era5 = ERA5Reanalysis.read_data(nc_file, lonlat)

total_mass = 1 - df_era5.ciwc.values - df_era5.clwc.values - df_era5.crcwc.values - df_era5.cswc.values
denice = df_era5.ciwc.values * (1/total_mass) * \
    kgkg_to_kgm3(df_era5.q.values * (1/total_mass),
                df_era5.p.values, df_era5.t.values) * 1000
denliq = df_era5.clwc.values * (1/total_mass) * \
    kgkg_to_kgm3(df_era5.q.values * (1/total_mass),
                df_era5.p.values, df_era5.t.values) * 1000

df_era5['denice'] = denice
df_era5['denliq'] = denliq

plt.plot(df_era5.denice, df_era5.p, label='CIWC')
plt.plot(df_era5.denliq, df_era5.p, label='CLWC')
plt.xlabel("$\text{g/m}^3$")
plt.ylabel("P [hPa]")
plt.gca().invert_yaxis()
plt.legend()
plt.grid()

df_era5.plot("o3", 'p',
            xlabel="$\text{O}_3$ [kg/kg]", ylabel="P [hPa]",
            grid=True, legend=False)

plt.gca().invert_yaxis()
```

Listing 3. Example code using PyRTLlib module to retrieve atmospheric profiles from the ERA5 Reanalysis.

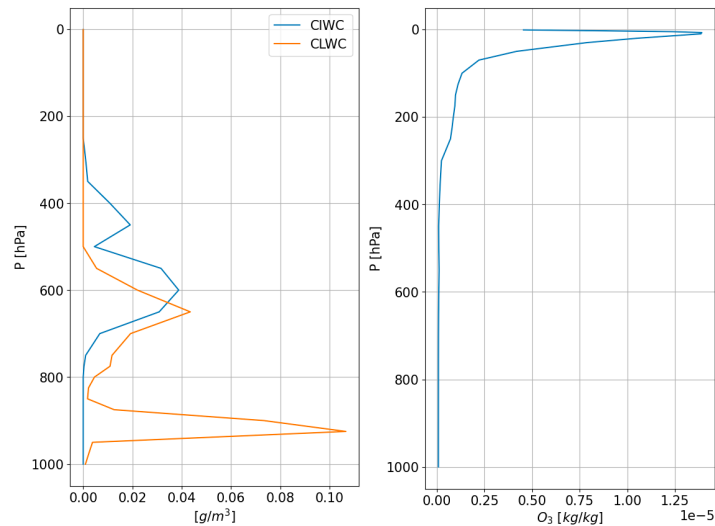


Figure 3. Graphical output of Listing 3, showing atmospheric profiles from ERA5 reanalysis for the nearest grid point to a location in Southern Italy (longitude 16.04°; latitude 39.44°) on 16 May 2023 at 18:00 UTC. Left: Cloud liquid water content (CLWC) and cloud ice water content (CIWC). Right: ozone mass mixing ratio.

4 Examples of applications

PyRTlib was developed to provide an educational RT software in Python, especially targeting students and younger scientists that mostly use this language for scientific code development. For this reason, PyRTlib was built with additional modules for facilitating the retrieval and management of popular datasets as input, such as radiosonde repository or global reanalysis, as shown in Section 3. This makes PyRTlib a useful end-to-end RT tool for pedagogical purposes, being flexible and interactive with easy access to all kinds of intermediate variables (e.g., absorption, optical depth, opacity, mean radiating temperature) (Table 4.1 and 4.2). In addition, PyRTlib was designed to allow easy comparison of MW RT calculations using a set of atmospheric absorption models proposed throughout the last three decades, for any platform (ground-based, airborne, and spaceborne) and observing geometry (zenith, nadir, slant). Finally, PyRTlib implements a general rigorous approach to estimate the uncertainty related to the absorption model (Cimini et al., 2018; Gallucci et al., 2023) and thus it provides T_B calculations with the associated uncertainty estimate, to our knowledge a unique feature in the MW RT scenario. In the following, few examples of applications are given, together with the output figure and the simple code for obtaining it.

Table 4.1: Output variables from PyRTlib.

Variable	Description	Units
tbtotal	brightness temperature includes cosmic background	K
tbatm	atmospheric brightness temperature, no cosmic	K
tmr	mean radiating temperature of the atmosphere	K

tmrclid	mean radiating temperature of the lowest cloud layer	K
taudry	dry air absorption integrated over each ray path	Np
tauwet	water vapor absorption integrated over each ray path	Np
tauliq	cloud liquid absorption integrated over each ray path	Np
tauice	cloud ice absorption integrated over each ray path	Np

Table 4.2: List of all the intermediate variables accessible from PyRTlib.

Variable	Description	Units
taulaydry	dry air absorption integrated over each ray path	Np
taulaywet	water vapor absorption integrated over each ray path	Np
taulayliq	cloud liquid absorption integrated over each ray path	Np
taulayice	cloud ice absorption integrated over each ray path	Np
srho	water vapor density integrated along each ray path	cm
swet	wet refractivity integrated along each ray path	cm
sdry	dry refractivity integrated along each ray path	cm
sliq	cloud ice density integrated along each ray	cm
sice	cloud liquid density integrated along each ray	cm

510

4.1 Simulation of downwelling T_B

As a first example, we propose the simulation of downwelling T_B spectra in a typical MW spectral range. This simple example may turn useful to simulate the measurements from a multi-channel ground-based microwave radiometer, e.g. those widely deployed in atmospheric profiling observatories (Rüfenacht et al., 2021; Shrestha et al., 2022). As input, the user can opt for one of the six climatological atmospheric profiles predefined in PyRTlib (from Anderson et al., 1986: TROPICAL, MIDLAT WINTER, MIDLAT SUMMER, ARCTIC WINTER, ARCTIC SUMMER, US STANDARD) or any of the radiosonde/reanalysis profiles retrieved from the repositories introduced in Section 3. Listing 4 shows the code to compute and plot downwelling T_B spectra at 1-GHz frequency resolution for two typical climatology conditions (tropical and subarctic winter), each at two pointing angles (90° and 30° elevation angle). The graphic output, reported in Figure 4, shows the typical peaks corresponding to resonant absorption of atmospheric gases (O_2 at 50-70 and 118 GHz, H_2O at 22.2 and 183 GHz) as well as the non-resonant continuum absorption due to H_2O (monotonically increasing with frequency). The peaks and the continuum show the emission added by the atmospheric gases with respect to the relatively cold emission coming from the outer boundary of the atmosphere (the so called cosmic background). T_B spectra are generally higher for tropical conditions, due to higher atmospheric temperature and humidity with respect to subarctic winter, and for lower elevation angles, due to the slant longer path travelled by radiation throughout the atmosphere.

515

520

525

```

from pyrtlib.tb_spectrum import TbCloudRTE
from pyrtlib.climatology import AtmosphericProfiles as atmp
from pyrtlib.utils import ppmv2gkg, mr2rh

```

```

colors = ['#ff0405', '#0404ff', '#0fff0e', '#000000']
atms = [atmp.TROPICAL, atmp.SUBARCTIC_WINTER]
cnt = 0
for atm in atms:
    z, p, _, t, md = atmp.g1_atm(atm)
    gkg = ppmv2gkg(md[:, atmp.H2O], atmp.H2O)
    rh = mr2rh(p, t, gkg)[0] / 100
    frq = np.arange(20, 201, 1)
    ang = np.array([90., 30.])

    for a in ang:
        rte = TbCloudRTE(z, p, t, rh, frq, np.array([a]))
        rte.init_absmdl('R19SD')
        rte.satellite = False
        df = rte.execute()
        df = df.set_index(frq)
        df.tbtotal.plot(figsize=(12,8), xlabel="Frequency [GHz]", ylabel="Brightness Temperature [K]",
                        label=atmp.atm_profiles()[atm] + ' (' + str(a) + '°)', lw=3, legend=True,
                        color=colors[cnt], grid=True)

    cnt += 1

```

Listing 4. Example code using PyRTLlib module to calculate downwelling T_B in the 20 to 201 GHz spectral range (1 GHz resolution) using two predefined climatological profiles (Tropical and Subarctic Winter) at 90° and 30° elevation angles.

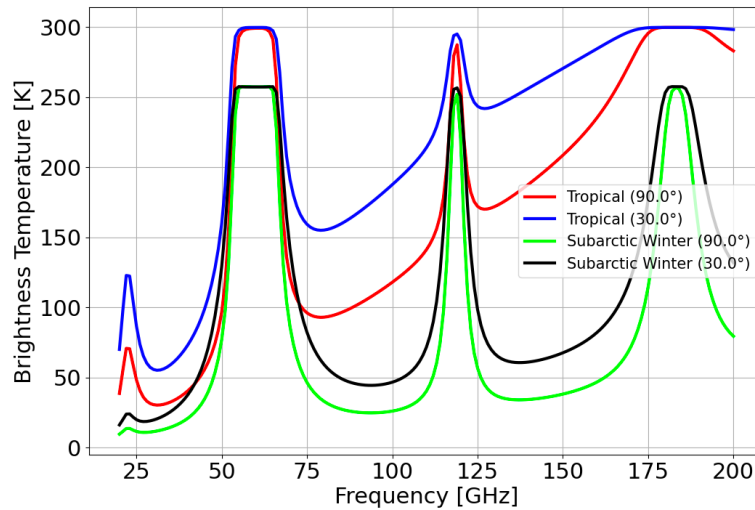


Figure 4. Graphical output of Listing 4, showing downwelling T_B spectra computed for two typical climatologies (Tropical and Subarctic Winter) at two elevation angles (90° and 30°).

4.2 Simulation of upwelling T_B

The second example shows the simulation of upwelling T_B spectra, as those typically sampled by satellite-based MW radiometers (e.g., Moradi et al., 2015). Listing 5 shows the code to compute and plot upwelling T_B spectra at 1-GHz frequency resolution for typical mid-latitude summer climatology conditions. The graphic output is reported in Figure 5, where the impact of pointing angle and surface emissivity is shown by varying their values. In particular, 90° pointing angle indicates nadir

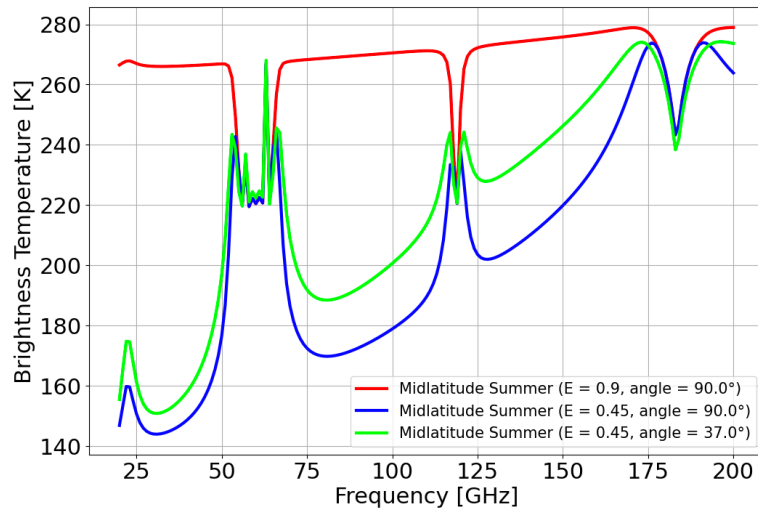
540 observations, while 37° indicates typical observing angle of MW imagers (53° from nadir), while 0.9 and 0.45 represent typical high and low emissivity values in the MW spectral region. Figure 5 shows that if the emissivity is relatively high (e.g., 0.9), the spectrum resembles that of a warm black-body emission at ~ 270 K (except where strong atmospheric absorption occurs, e.g., 60, 118, and 183 GHz). Conversely, if the emissivity is relatively low (e.g., 0.45), the background is relatively cold and the atmospheric emission features stick out, similarly to Figure 4. However, near the center of strong emission features (e.g., 60, 118, and 183 GHz) T_B appears flipped with respect to Figure 4, indicating gas absorption that removes radiation from the emission coming from the relatively warm background. It is notable that in those regions T_B nearly overlap for the three emissivity and angle conditions; this is because the atmospheric opacity is so high to make T_B saturate within a short distance, thus becoming insensitive to surface emission and observing angle (i.e., path length). PyRTLlib also allows frequency-dependent surface emissivity to be provided in input.

545

```
z, p, _, t, md = atmp.gl_atm(atmp.MIDLATITUDE_SUMMER)
gkg = ppmv2gkg(md[:, atmp.H2O], atmp.H2O)
rh = mr2rh(p, t, gkg)[0] / 100
frq = np.arange(20, 201, 1)
ang = np.array([90., 37.])

colors = ['#ff0405', '#0404ff', '#0fff0e']
cnt = 0
for a in ang:
    rte = TbCloudRTE(z, p, t, rh, frq, np.array([a]))
    rte.init_absmdl('R19SD')
    for e in [0.9, 0.45]:
        if a == 37. and e == 0.90:
            continue
        rte.emissivity = e
        df = rte.execute()
        df = df.set_index(frq)
        df.tbtotal.plot(figsize=(12,8), xlabel="Frequency [GHz]", ylabel="Brightness Temperature [K]",
                        label=atmp.atm_profiles()[atmp.MIDLATITUDE_SUMMER] + ' (E = ' + str(e) + ', angle = ' +
str(a) + '°)',
                        color=colors[cnt], lw=3, legend=True, grid=True)
        cnt += 1
```

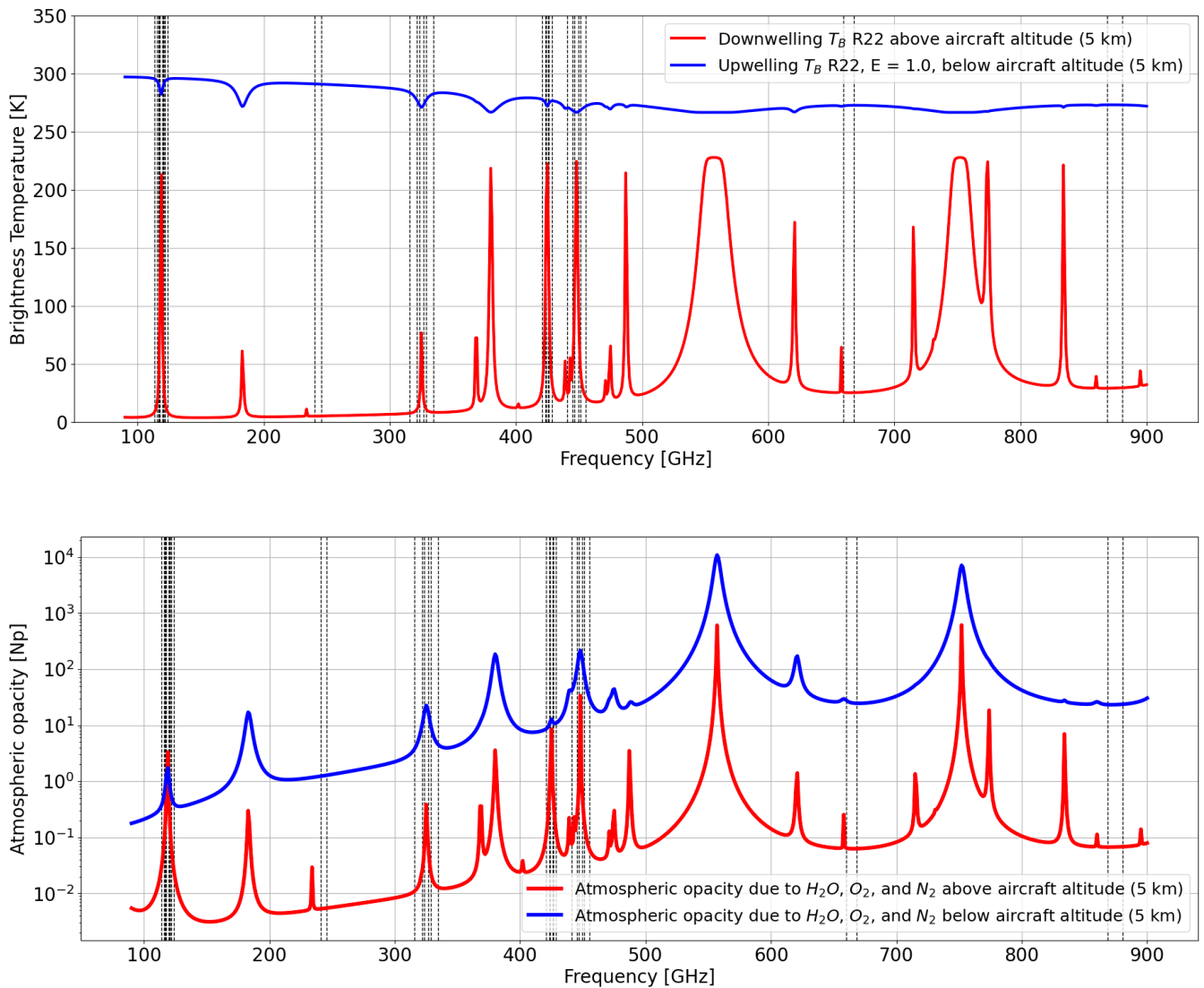
Listing 5. Example code using PyRTLlib module to calculate upwelling T_B in the 20 to 201 GHz spectral range (1 GHz resolution) using a predefined climatological profile (Midlatitude Summer) at 90° and 37° elevation angle with constant surface emissivity values of 0.9 and 0.45.



550 **Figure 5.** Graphical output of Listing 5, showing upwelling T_B spectra computed for a predefined climatological profile (Midlatitude Summer) at 90° and 37° elevation angles with constant surface emissivity values of 0.9 and 0.45.

4.3 Simulation of simultaneous downwelling and upwelling T_B

Simultaneous observations of downwelling and upwelling T_B are typically performed from airborne scanning instruments that can alternate uplooking and downlooking views (e.g., Fox et al., 2017; Wang et al., 2017). Both views can be simulated by
 555 PyRTlib using the same atmospheric profile in input and specifying the altitude of the aircraft and the observing angle. Figure 6 shows the downwelling and upwelling T_B simulated assuming the aircraft at 5 km altitude looking down at nadir and up at zenith. The input profile comes from a radiosonde launched from Camborne (UK) at 12:00 UTC on 22 July 2021 and retrieved from the Wyoming Upper Air Archive, corresponding to location and period of experimental flights by the Facility for Airborne Atmospheric Measurements (FAAM) BAe-146 aircraft mounting the International Submillimetre Airborne Radiometer (ISMAR, Fox et al., 2017). ISMAR has 17 channels spanning the 118 to 874 GHz range, being developed as an
 560 airborne demonstrator for the Ice Cloud Imager (ICI), planned for the second generation of European polar-orbiting satellites (MetOp-SG) to be launched 2024 onwards. Note that PyRTlib functions allow to display and investigate not only T_B but all the intermediate RT variables, such as absorption, optical depth, opacity. For example, Figure 6 shows the atmospheric opacity above and below the aircraft as computed for the uplooking and downlooking views. Atmospheric absorption spectra from
 565 PyRTlib were compared with those computed with ARTS using the equivalent absorption model, resulting in differences within 0.05%, which are attributed to different assumptions in the variation of absorption coefficient across an atmospheric layer (Fox et al., 2023).



570

Figure 6. Top: downwelling and upwelling T_B simulating aircraft observations at respectively zenith and nadir from 5 km altitude (gas absorption model: R22; surface emissivity equal to 1). Bottom: Atmospheric opacity (τ) corresponding to dominant gases (H_2O , O_2 , and N_2) computed for the uplooking and downlooking views. All the features correspond to H_2O absorption but the following, due to O_2 : 118, 368, 424, 487, 715, 773, 834 GHz. Input profile from the radiosonde launched from Camborne (UK) on 22 July 2021 at 12:00 UTC and retrieved from the Wyoming Upper Air Archive. Vertical black lines indicate the ISMAR channel frequencies.

575

4.4 Comparison of absorption models

The PyRTlib package allows T_B simulations with different versions of atmospheric gas absorption models. As mentioned earlier, the spectroscopy underlying absorption models is continuously updated, following the latest findings from laboratory and field campaign experiments. Currently, PyRTlib implements absorption routines originally based on the MPM code (Liebe, 1989) with spectroscopy modified throughout the last decades. Specifically, the following versions are readily callable in PyRTlib (with reference to the paper that motivated the update, where available): R98 (Rosenkranz, 1998); R03 (Tretyakov et al., 2003), R16, R17 (Rosenkranz, 2017), R19, R19SD (Rosenkranz and Cimini, 2019), R20, R20SD (Makarov et al., 2020), R21SD (Koshelev et al., 2021), until R22SD (Koshelev et al., 2022). The original Fortran code for most of these absorption routines by P. W. Rosenkranz are freely accessible through a repository (http://cetemps.aquila.infn.it/mwrnet/lblmrt_ns.html). In the following, we present an example in which the latest version at the time of writing, R22SD, is compared with R98, which still represents a widely used model (e.g., Picard et al., 2009). Modifications in R22SD with respect to R98 include: updated line width at 22 GHz (Payne et al., 2008), updated water vapor continuum coefficients scaled after Turner et al. (2009), revised O_2 mixing coefficients for 50-70 GHz and 118 GHz lines (Makarov et al., 2020), speed-dependent line shape for the water vapor absorption lines at 22 (Rosenkranz and Cimini, 2019) and 183 GHz (Koshelev et al., 2021), addition of four submillimeter-wave water vapor lines (860, 970, 987, 1097 GHz), and other updated line parameters taken from the most recent release of the HITRAN database (HITRAN2020). To test two gas absorption versions, a simple observation minus simulation (O-S) approach can be used, exploiting MW ground-based remote sensing and balloon-borne sounding measurements from the US Department of Energy (DOE) Atmospheric Radiation Measurement (ARM) program (<https://arm.gov>), which can be freely accessed from the ARM data center (<https://adc.arm.gov>). In fact, ARM deploys a network of ground-based MW radiometers (MWR) across its observatory sites (Cadeddu et al., 2013; Cadeddu & Liljegren, 2018). These instruments measure downwelling T_B at selected frequency channels under all-sky conditions. From the same sites, ARM regularly launches radiosondes; the ARM balloon-borne sounding system (BBSS) products provide profiles of in situ measurements of atmospheric pressure, temperature, humidity, as well as wind speed and direction (Holdridge, 2020), which can be given in input to PyRTlib to simulate zenith downwelling T_B . A dataset of colocated and nearly simultaneous MWR observations and RT simulations can be then used to test and validate simulations from different absorption models. Such a dataset was retrieved from the deployment of the ARM mobile facility in Highland Center, Cape Cod (MA, USA) during the two-column aerosol project (TCAP) in 2012 (Titos et al., 2014). The observations are the T_B measured by a MWR profiler (MWRP). The MWRP product provides measurements of T_B at 12 frequency channels in the range from 22 to 58 GHz. Frequencies between 22 and 52 GHz are mostly sensitive to atmospheric water vapor and cloud liquid, while frequencies between 51 and 60 GHz are sensitive to atmospheric temperature through the absorption of atmospheric oxygen. Simulations at the same frequency channels are computed from the 4-daily radiosondes (at 05:30, 11:30, 17:30, and 23:30 UTC) launched during TCAP and processed by PyRTlib. To avoid spatial-temporal uncertainty of clouds, the comparison is made in clear-sky conditions, applying a cloud screening to both radiosonde and MWRP data. Clear-sky conditions were selected using a relative

610 humidity threshold, specifically rejecting radiosondes with at least four pressure levels with relative humidity higher than 95% (Clain et al., 2015). Furthermore, an observation-based screening was applied, removing data for which 1-h standard deviation of the T_B at 30 GHz was larger than 0.5 K, indicating possible obstructions or cloud contamination (De Angelis et al., 2017). From a total of 592 radiosonde, these two screenings leave 149 match-ups for the analysis. Simulated and observed datasets were compared by selecting and averaging MWRP observations falling within -45 minute/+1 hour from each radiosonde
 615 launch time, so as to reduce the temporal-spatial mismatch with respect to the radiosonde measurements. The result of the comparison of R98 and R22 models versus the observed dataset is shown in Figures 7 and 8.

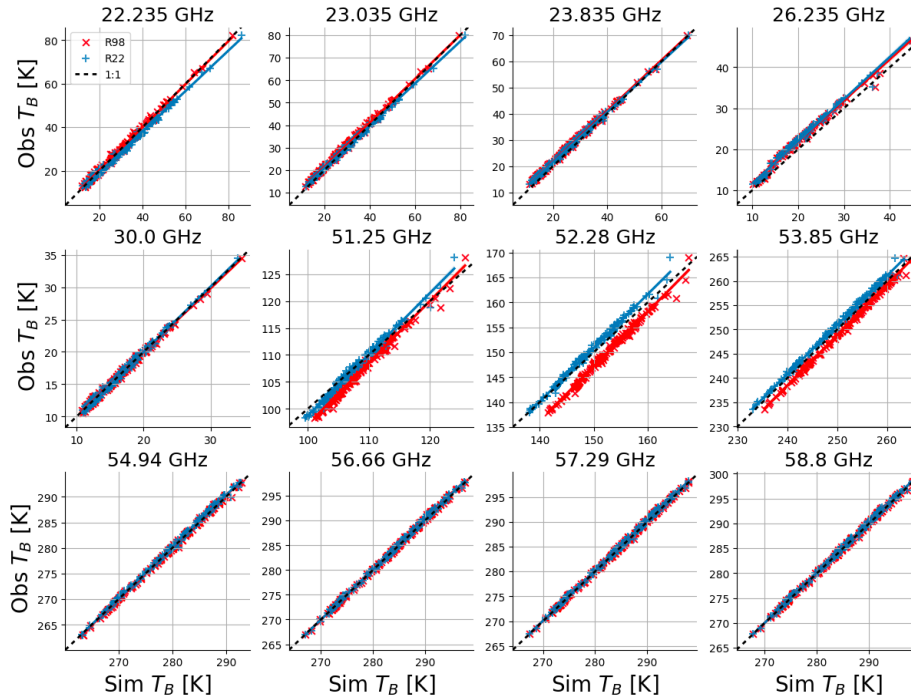


Figure 7. Scatter plots of downwelling T_B as observed by a MWRP (y-axis) and simulated with PyRTlib (x-axis) using two versions of the gas absorption model (R98 in red x and R22 in blue +). Each panel shows one MWRP channel. Markers show
 620 149 MWRP-radiosonde match-ups in clear sky selected from a 6-month period during the TCAP campaign. MWRP and radiosonde data were retrieved from the ARM data center (Cadeddu and Gibler, 2012; Keeler and Burk, 2012).

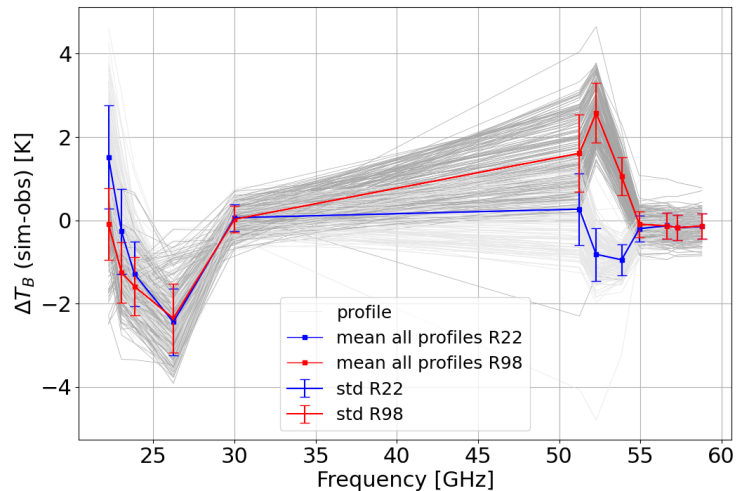


Figure 8. Spectrum of simulations minus observations statistics from the 149 MWRP-radiosonde match-ups in clear sky dataset in Figure 7. Simulations computed using R98 are shown in red, while using R22 in blue. Dots and bars indicate respectively the mean value and the standard deviation over the whole dataset.

Figure 7 shows that RT simulations with both absorption models tend to align with observed TB over the whole range of variations for all MWRP channels, although larger differences are evident at 51-54 GHz for R98. Bias of the same order of magnitude for the 51–54 GHz channels were previously reported for the R98 model employing MWR of different types and manufacturers (e.g., Löhnert and Maier, 2012; De Angelis et al., 2017). De Angelis et al. (2017) attribute these to a combination of systematic uncertainties stemming from inaccurate instrument bandpass characterization, instrument calibration, and absorption model. Since then, two major updates have been proposed for the O₂ spectroscopic parameters in this range (mainly mixing coefficients) from laboratory experiments (Tretyakov et al., 2005; Makarov et al., 2020), the latest of which is implemented in R22. Figure 8 reports mean and standard deviation of the simulation minus observation differences, which indicate better performances for R22 with respect to R98 in modelling T_B for channels along the low-frequency wing of the O₂ absorption complex, confirming recent independent results (Belikovich et al., 2021; 2022). Unexpectedly, Figure 8 also indicates differences ~2 K for R22 at 22.2 and 26.235 GHz channels, which will be discussed in next Section. PyRTlib also allows quantifying the impact on T_B of the most recent set of O₂ spectroscopic parameters (Makarov et al., 2020) with respect to the previous one (Tretyakov et al., 2005). In fact, two absorption model versions implemented in PyRTlib, namely R19 and R22, only differ by this aspect in the 50-70 GHz range, and thus the T_B impact is simply evaluated by computing T_B with these two versions and taking the difference. To make it general, we evaluate the impact by processing the set of 83 diverse atmospheric profiles commonly used to train RTTOV (Saunders et al, 2018). This profile set was carefully chosen from more than 100 million profiles to represent a realistic range of possible diverse atmospheric conditions (Matricardi, 2008) and it is openly available through the Numerical Weather Prediction Satellite Application Facility (NWPSAF) (<https://nwp-saf.eumetsat.int/site/software/atmospheric-profile-data/>). Figure 9 shows the differences between the two models for the

downwelling and upwelling T_B simulated at 50 MHz resolution from the 83 diverse profiles, together with the mean difference and standard deviation (std). For downwelling T_B , the updated O_2 mixing coefficients proposed by Makarov et al. (2020) decrease T_B with respect to the previous ones (Tretyakov et al., 2005) by up to 4-5 K on average, peaking at 53 and 66 GHz, with an estimated global variability ~ 1 K (1-sigma). For upwelling T_B , the situation is opposite, with a decrease up to -0.6 K with 0.2 K std, although it depends on the assumed surface emissivity (set to 1 in this example).

650

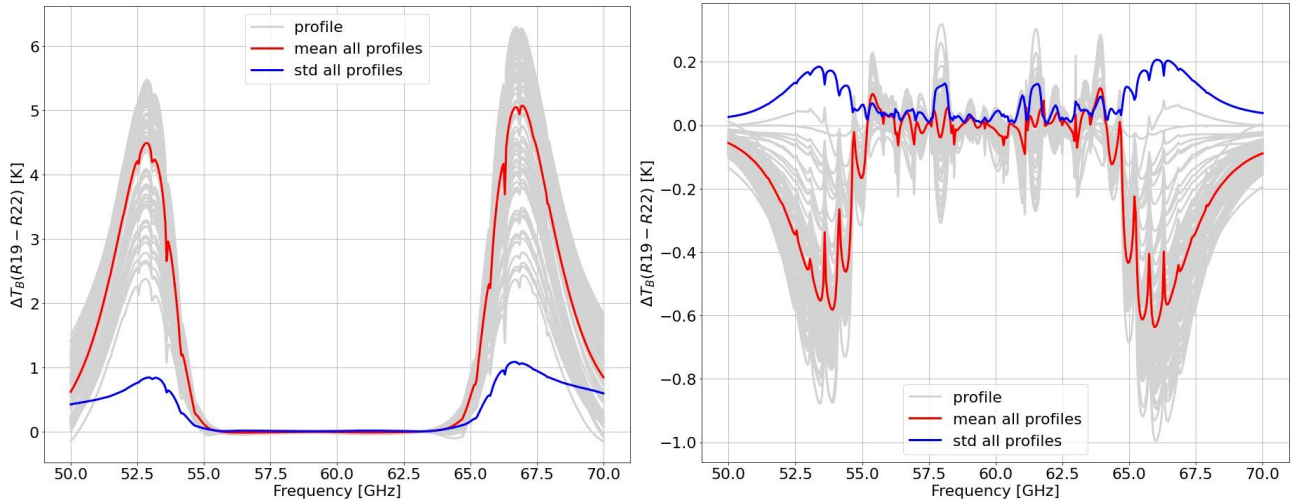


Figure 9. Differences of downwelling (left) and upwelling (right) T_B computed with R19 and R22 absorption models at 50 MHz resolution for the set of NWPSAF 83 diverse profiles. Red and blue lines indicate mean difference and standard deviation of the dataset. Upwelling simulations assume constant surface emissivity equal to 1.

655

4.5 Absorption model uncertainty

RT calculations depend on absorption models and the underlying spectroscopic parameters. The values of these parameters are determined through theoretical assumptions or analysis of laboratory or field data, and thus are inherently affected by uncertainty. The uncertainty affecting the spectroscopic parameters contributes to the uncertainty of the absorption, which affects the RT calculations, and in turn the retrieval of atmospheric variables from remotely sensed observations (Cimini et al., 2018). PyRTlib allows to compute the sensitivity of RT calculations to the uncertainty of various spectroscopic parameters, defined as the T_B difference (ΔT_B) obtained by perturbing the value of spectroscopic parameter by its uncertainty. Figure 10 reports the sensitivity of zenith downwelling T_B to two water vapor absorption spectroscopic parameters, namely the line intensity (S) at 22.2 GHz and the foreign continuum coefficient (C_f), showing similar results as in the original study (Cimini et al., 2018, Figure 2). In addition to the uncertainty of individual parameters, the correlation between the uncertainty on various parameters must also be taken into account, and therefore it is necessary to calculate the complete uncertainty covariance matrix (Rosenkranz, 2005). A general and rigorous approach to estimate the uncertainty covariance matrix for MW absorption models has been outlined (Rosenkranz et al.,

665

2018) and applied to the simulations of downwelling (Cimini et al., 2018) and upwelling (Gallucci et al., 2023) radiation.

670 The full uncertainty covariance matrix from Cimini et al. (2018) is accessible through the PyRTlib code, as well as
supplement files of the original paper ([https://acp.copernicus.org/articles/18/15231/2018/acp-18-15231-2018-](https://acp.copernicus.org/articles/18/15231/2018/acp-18-15231-2018-supplement.zip)
supplement.zip). PyRTlib inherits this development and provides tools to compute T_B together with the associated
uncertainty estimate. One example is shown in Figure 11. It shows ground-based zenith radiometric measurements from
the MWRP with its typical calibration uncertainty (Cadeddu & Liljegren, 2018) compared with zenith downwelling T_B
675 computed processing one radiosonde from the TCAP dataset, together with the associated uncertainty estimate $\sigma(T_B)$.
 $\sigma(T_B)$ is computed within PyRTlib by propagating the spectroscopic parameter uncertainty through the radiative transfer.
Calling $\mathbf{Cov}(p)$ the parameter uncertainty covariance matrix (as in Cimini et al., 2018), \mathbf{K}_p the sensitivity of T_B to
spectroscopic parameter (Jacobian), $\sigma(T_B)$ is computed as

$$\sigma^2(T_B) = \text{diag}(\mathbf{Cov}(T_B)) = \text{diag}(\mathbf{K}_p \cdot \mathbf{Cov}(p) \cdot \mathbf{K}_p^T)$$

680 where T indicates the matrix transpose. PyRTlib computes the Jacobians \mathbf{K}_p by the brute force method and provides in output
the full covariance matrix of T_B uncertainty $\mathbf{Cov}(T_B)$. Figure 11 reports the square-root of the diagonal terms (i.e., $\sigma(T_B)$),
showing that for this single case the observation minus simulation differences fit within the overlap of instrumental calibration
uncertainty and absorption model uncertainty at 3-sigma, and for some channels, at 1-sigma level. The only channel that is
nearly off is the 26.235 GHz. This happens also for other radiosondes and absorption models, as evident in Figure 8, suggesting
685 that the calibration of this particular channel is questionable and may need recalibration service.

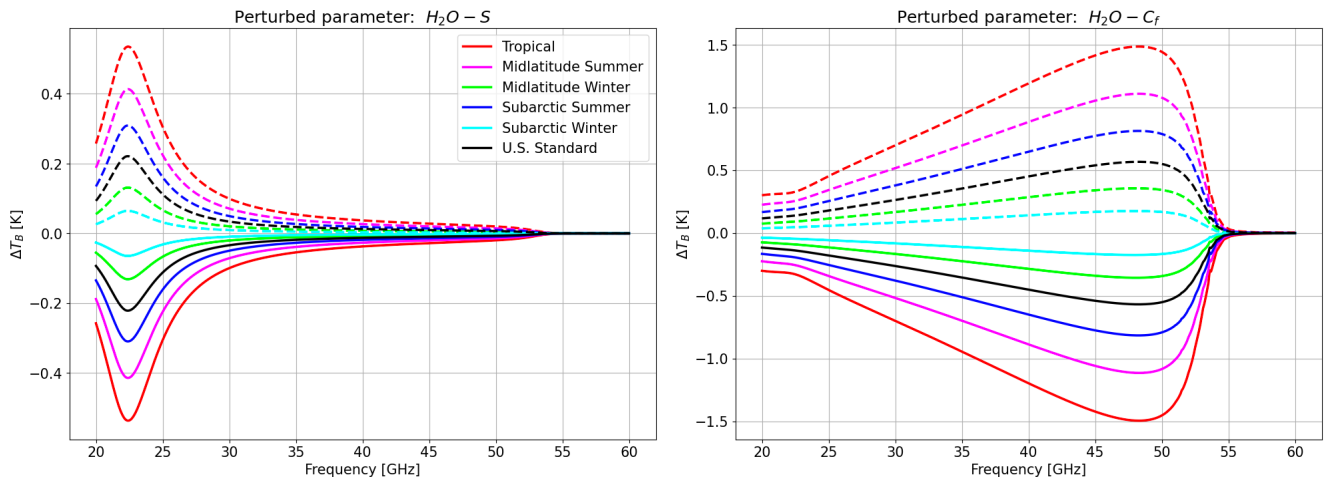


Figure 10. Sensitivity of zenith downwelling T_B to water vapor absorption parameters, computed at 0.1 GHz spectral
resolution. Left: line intensity (S) at 22 GHz. Right: foreign continuum coefficient (C_f). Solid lines correspond to negative
perturbation (value - uncertainty), while dashed lines correspond to positive perturbation (value + uncertainty). Different
690 colors indicate six typical climatological conditions. Adapted from Cimini et al., 2018.

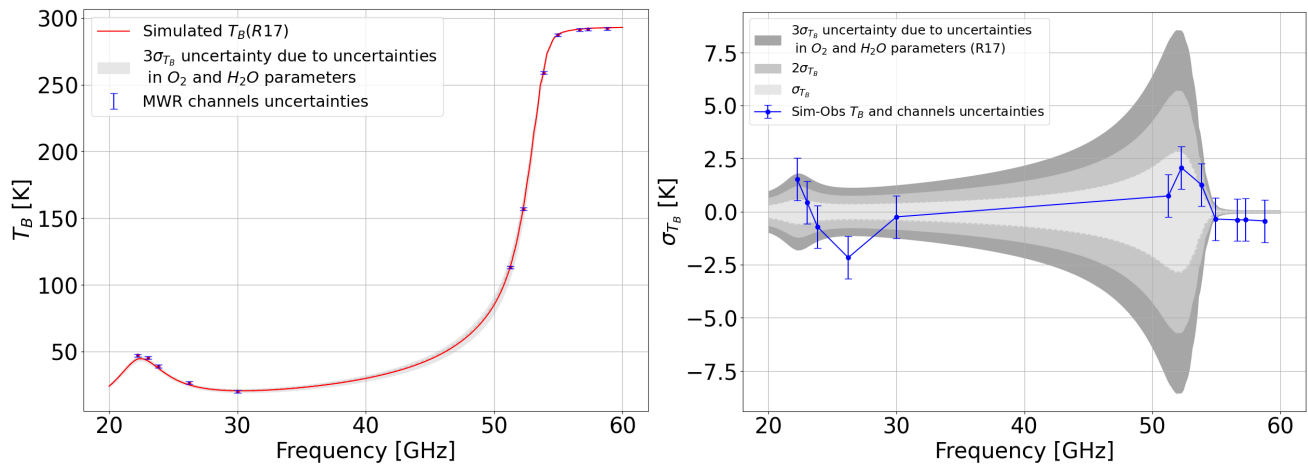


Figure 11. Left: Zenith downwelling T_B spectrum (red line) computed from one radiosonde launched from the ARM mobile facility during TCAP, Cape Cod, MA, USA (2012-08-26 16:58 UTC). Blue points and bars indicate the nearly simultaneous measurements from the colocated MWRP at 12 frequency channels and their calibration uncertainty. Right: Simulations minus observations at the 12 channels (blue points) with the instrumental calibration uncertainty (blue bars), together with the estimated uncertainty for zenith downwelling T_B ($\sigma(T_B)$) due to the uncertainty in absorption model spectroscopic parameters (at 1-, 2-, and 3-sigma levels).

5 Summary and future developments

This paper presents PyRTlib version 1.0, a Python library for non-scattering atmospheric microwave radiative transfer computations. The intention for PyRTlib is to provide a user-friendly tool for computing down and up-welling brightness temperatures and related quantities (e.g., atmospheric absorption, optical depth, opacity) in Python, a flexible language that nowadays represents the most used for scientific software development, especially by students and early career scientists. Within its limits, mainly non scattering and 1-D geometry, PyRTlib allows simulating observations from ground-based, airborne, and satellite microwave sensors in clear sky and in cloudy conditions (under Rayleigh approximation). Clearly, the intention for PyRTlib is not to be a competitor for other radiative transfer codes that excel for computational efficiency (RTTOV, CRTM), flexibility (ARTS), modularity (ARTS, Py4CATS), and applicability (ARTS, PAMTRA). Nevertheless, despite the speed limitations and the omission of important aspects of RT (e.g., spherical geometry and particle scattering), we believe PyRTlib is attractive as an educational tool because of the flexibility and ease of use, providing a quick interface to popular repositories of atmospheric profiles from radiosondes and model reanalysis. PyRTlib also allows peculiar investigations such as absorption model comparison and validation against observations (e.g., Section 4.4) and the estimation of brightness temperature uncertainty due to atmospheric absorption model (e.g., Section 4.5). In addition, PyRTlib could be used as a module for other Python codes that need atmospheric radiative transfer, e.g. the Snow Microwave Radiative Transfer

715 model (SMRT, Picard et al. 2018). Future developments include the implementation of (i) new absorption models (e.g. R23
came out at the time of submission), (ii) sensor-oriented calculations considering channels' spectral response functions, (iii)
uncertainty estimate for higher frequency brightness temperature calculations, as recently investigated (Gallucci et al., 2023),
(iv) additional tools for extrapolating the input profiles (e.g., Annex 3 of ITU-R P.835-6), (v) calculation of weighting
functions, (vi) additional tools for accessing other atmospheric data open repositories to be used as RT calculations input, e.g.,
720 the ARM data center and the Global Climate Observing System Reference Upper Air Network (GRUAN, Bodeker et al.,
2016).

6 Code and data availability

PyRTlib is available as a python package to users under an open-source GPL v3 license and it is free of charge. PyRTlib may
be obtained from the github repository <https://github.com/SatCloP/pyrtlib> or from the Zenodo repository
<https://doi.org/10.5281/zenodo.8219145>. Instructions for installing and running PyRTlib are provided in the PyRTlib User
725 Guide Documentation available at <https://satclp.github.io/pyrtlib>. The user documentation is rich in content and includes a
large number of examples on how to run and configure PyRTlib. The python package also includes scripts and test suite to
verify the installation and Jupyter Notebook examples for running the PyRTlib modules to be easily performed in your work
environment. PyRTlib is designed for multiplatform systems (UNIX/Linux, MacOS, Windows) and can be installed on any
computer supporting Python 3.8 (or higher) to work properly.

730 7 Competing interests

The contact author has declared that none of the authors has any competing interests.

8 Acknowledgements

735 The authors acknowledge the support of EUMETSAT through the ISMAR study (contract EUM/CO/20/4600002477/VM) and
the VICIRS study (contract EUM/CO/22/4600002714/FDA). The authors also acknowledge the support of ESA through the
REFDAT4ESAMWR project (contract 4000134771/21/NL/MG/mkn). PyRTlib development was also stimulated through the
COST Action CA18235 PROBE, supported by COST (European Cooperation in Science and Technology,
<https://www.cost.eu/>). The authors acknowledge the advice of Phil W. Rosenkranz (MIT, retired) and Stuart Fox (MetOffice)
throughout the software development.

740 *Author contributions.* SL, DC, and DG designed the research, contributed to data processing and analysis, and wrote the original manuscript. SL and DC developed the software with support from all co-authors. FR contributed to validation data analysis. All the co-authors helped to revise the manuscript.

References

745 Anderson, G. P., Clough, S. A., Kneizys, F. X., Chetwynd, J. H., and Shettle, E. P.: AFGL atmospheric constituent profiles (0.120km), Unknown, 1986.

Anon: University of Wyoming Upper Air Archive, n.d.

Ayala Pelaez, S. and Deline, C.: pySMARTS: SMARTS Python Wrapper (Simple Model of the Atmospheric Radiative Transfer of Sunshine), , <https://doi.org/10.11578/DC.20210816.1>, 2020.

750 Bauer, P., Geer, A. J., Lopez, P., and Salmond, D.: Direct 4D-Var assimilation of all-sky radiances. Part I: Implementation, *Quarterly Journal of the Royal Meteorological Society*, 136, 1868–1885, <https://doi.org/10.1002/qj.659>, 2010.

755 Belikovich, M. V., Kulikov, M. Y., Makarov, D. S., Skalyga, N. K., Ryskin, V. G., Shvetsov, A. A., Krasil'nikov, A. A., Dementyeva, S. O., Serov, E. A., and Feigin, A. M.: Long-Term Observations of Microwave Brightness Temperatures over a Metropolitan Area: Comparison of Radiometric Data and Spectra Simulated with the Use of Radiosonde Measurements, *Remote Sensing*, 13, 2061, <https://doi.org/10.3390/rs13112061>, 2021.

Belikovich, M. V., Makarov, D. S., Serov, E. A., Kulikov, M. Y., and Feigin, A. M.: Validation of Atmospheric Absorption Models within the 20–60 GHz Band by Simultaneous Radiosonde and Microwave Observations: The Advantage of Using ECS Formalism, *Remote Sensing*, 14, 6042, <https://doi.org/10.3390/rs14236042>, 2022.

760 Berk, A., Conforti, P., Kennett, R., Perkins, T., Hawes, F., and Bosch, J. van den: MODTRAN6: a major upgrade of the MODTRAN radiative transfer code, in: Algorithms and Technologies for Multispectral, Hyperspectral, and Ultraspectral Imagery XX, Algorithms and Technologies for Multispectral, Hyperspectral, and Ultraspectral Imagery XX, 113–119, <https://doi.org/10.1117/12.2050433>, 2014.

765 Bodeker, G. E., Bojinski, S., Cimini, D., Dirksen, R. J., Haeffelin, M., Hannigan, J. W., Hurst, D. F., Leblanc, T., Madonna, F., Maturilli, M., Mikalsen, A. C., Philipona, R., Reale, T., Seidel, D. J., Tan, D. G. H., Thorne, P. W., Vömel, H., and Wang, J.: Reference Upper-Air Observations for Climate: From Concept to Reality, *Bulletin of the American Meteorological Society*, 97, 123–135, <https://doi.org/10.1175/BAMS-D-14-00072.1>, 2016.

770 Boukabara, S.-A., Garrett, K., Grassotti, C., Iturbide-Sanchez, F., Chen, W., Jiang, Z., Clough, S. A., Zhan, X., Liang, P., Liu, Q., Islam, T., Zubko, V., and Mims, A.: A physical approach for a simultaneous retrieval of sounding, surface, hydrometeor, and cryospheric parameters from SNPP/ATMS, *Journal of Geophysical Research: Atmospheres*, 118, 12,600–12,619, <https://doi.org/10.1002/2013JD020448>, 2013.

- Buehler, S. A., Eriksson, P., Kuhn, T., von Engeln, A., and Verdes, C.: ARTS, the atmospheric radiative transfer simulator, *Journal of Quantitative Spectroscopy and Radiative Transfer*, 91, 65–93, <https://doi.org/10.1016/j.jqsrt.2004.05.051>, 2005.
- 775 Buehler, S. A., Defer, E., Evans, F., Eliasson, S., Mendrok, J., Eriksson, P., Lee, C., Jiménez, C., Prigent, C., Crewell, S., Kasai, Y., Bennartz, R., and Gasiewski, A. J.: Observing ice clouds in the submillimeter spectral range: the CloudIce mission proposal for ESA’s Earth Explorer 8, *Atmospheric Measurement Techniques*, 5, 1529–1549, <https://doi.org/10.5194/amt-5-1529-2012>, 2012.
- Buehler, S. A., Mendrok, J., Eriksson, P., Perrin, A., Larsson, R., and Lemke, O.: ARTS, the Atmospheric Radiative Transfer Simulator – version 2.2, the planetary toolbox edition, *Geoscientific Model Development*, 11, 1537–1556, <https://doi.org/10.5194/gmd-11-1537-2018>, 2018.
- 780
- Cadeddu, M. and Gibler, G.: Microwave Radiometer Profiler (MWRP), <https://doi.org/10.5439/1025254>, 2012.
- Cadeddu, M. P. and Liljegren, J.: Microwave Radiometer Profiler (MWRP) Instrument Handbook, <https://doi.org/10.2172/1424403>, 2018.
- 785
- Cadeddu, M. P., Payne, V. H., Clough, S. A., Cady-Pereira, K., and Liljegren, J. C.: Effect of the Oxygen Line-Parameter Modeling on Temperature and Humidity Retrievals From Ground-Based Microwave Radiometers, *IEEE Transactions on Geoscience and Remote Sensing*, 45, 2216–2223, <https://doi.org/10.1109/TGRS.2007.894063>, 2007.
- Cadeddu, M. P., Liljegren, J. C., and Turner, D. D.: The Atmospheric radiation measurement (ARM) program network of microwave radiometers: instrumentation, data, and retrievals, *Atmospheric Measurement Techniques*, 6, 2359–2372, <https://doi.org/10.5194/amt-6-2359-2013>, 2013.
- 790
- Chapman, I. M., Naylor, D., Gom, B. G., Querel, R. R., and Davis-Imhof, P.: BTRAM : An Interactive Atmospheric Radiative Transfer Model, 2010.
- Cimini, D., Rosenkranz, P. W., Tretyakov, M. Y., Koshelev, M. A., and Romano, F.: Uncertainty of atmospheric microwave absorption model: impact on ground-based radiometer simulations and retrievals, *Atmospheric Chemistry and Physics*, 18, 15231–15259, <https://doi.org/10.5194/acp-18-15231-2018>, 2018.
- 795
- Cimini, D., Hocking, J., Angelis, F. D., Cersosimo, A., Paola, F. D., Gallucci, D., Gentile, S., Gerdali, E., Larosa, S., Nilo, S., Romano, F., Ricciardelli, E., Ripepi, E., Viggiano, M., Luini, L., Riva, C., Marzano, F. S., Martinet, P., Song, Y. Y., Ahn, M. H., and Rosenkranz, P. W.: RTTOV-gb v1.0 – updates on sensors, absorption models, uncertainty, and availability, *Geoscientific Model Development*, 12, 1833–1845, <https://doi.org/10.5194/gmd-12-1833-2019>, 2019.
- 800
- Cimini, D., Serio, C., Masiello, G., Mastro, P., Ricciardelli, E., Paola, F. D., Larosa, S., Gallucci, D., Hultberg, T., August, T., and Romano, F.: Spectrum Synergy for Investigating Cloud Microphysics, *Bulletin of the American Meteorological Society*, 104, E606–E622, <https://doi.org/10.1175/BAMS-D-22-0008.1>, 2023.

- 805 Clain, G., Brogniez, H., Payne, V. H., John, V. O., and Luo, M.: An Assessment of SAPHIR Calibration Using Quality Tropical Soundings, *Journal of Atmospheric and Oceanic Technology*, 32, 61–78, <https://doi.org/10.1175/JTECH-D-14-00054.1>, 2015.
- Clough, S. A., Shephard, M. W., Mlawer, E. J., Delamere, J. S., Iacono, M. J., Cady-Pereira, K., Boukabara, S., and Brown, P. D.: Atmospheric radiative transfer modeling: a summary of the AER codes, *Journal of Quantitative Spectroscopy and Radiative Transfer*, 91, 233–244, <https://doi.org/10.1016/j.jqsrt.2004.05.058>, 2005.
- 810 De Angelis, F., Cimini, D., Hocking, J., Martinet, P., and Kneifel, S.: RTTOV-gb – adapting the fast radiative transfer model RTTOV for the assimilation of ground-based microwave radiometer observations, *Geoscientific Model Development*, 9, 2721–2739, <https://doi.org/10.5194/gmd-9-2721-2016>, 2016.
- De Angelis, F., Cimini, D., Löhnert, U., Caumont, O., Haeefe, A., Pospichal, B., Martinet, P., Navas-Guzmán, F., Klein-Baltink, H., Dupont, J.-C., and Hocking, J.: Long-term observations minus background monitoring of ground-based brightness temperatures from a microwave radiometer network, *Atmospheric Measurement Techniques*, 10, 3947–3961, <https://doi.org/10.5194/amt-10-3947-2017>, 2017.
- 815 Ding, S., Yang, P., Weng, F., Liu, Q., Han, Y., van Delst, P., Li, J., and Baum, B.: Validation of the community radiative transfer model, *Journal of Quantitative Spectroscopy and Radiative Transfer*, 112, 1050–1064, <https://doi.org/10.1016/j.jqsrt.2010.11.009>, 2011.
- 820 Durre, I., Yin, X., Vose, R. S., Applequist, S., Arnfield, J., Korzeniewski, B., and Hundermark, B.: Integrated Global Radiosonde Archive (IGRA), Version 2, <https://doi.org/10.7289/V5X63K0Q>, 2016.
- Durre, I., Yin, X., Vose, R. S., Applequist, S., and Arnfield, J.: Enhancing the Data Coverage in the Integrated Global Radiosonde Archive, *Journal of Atmospheric and Oceanic Technology*, 35, 1753–1770, <https://doi.org/10.1175/JTECH-D-17-0223.1>, 2018.
- 825 Efremenko, D. S., Molina García, V., Pflug, B., and Trautmann, T.: PYDOME: python library for radiative transfer computations, in: *Living Planet Symposium 2019*, 2019.
- Eriksson, P., Jiménez, C., and Buehler, S. A.: Qpack, a general tool for instrument simulation and retrieval work, *Journal of Quantitative Spectroscopy and Radiative Transfer*, 91, 47–64, <https://doi.org/10.1016/j.jqsrt.2004.05.050>, 2005.
- 830 Eriksson, P., Buehler, S. A., Davis, C. P., Emde, C., and Lemke, O.: ARTS, the atmospheric radiative transfer simulator, version 2, *Journal of Quantitative Spectroscopy and Radiative Transfer*, 112, 1551–1558, <https://doi.org/10.1016/j.jqsrt.2011.03.001>, 2011.
- 835 ESA TN TEC-EEP/2016.184/AM, Tropospheric Media Calibration System for accurate ranging of space science missions - Definitions of parameters and test procedures for assessment of instrument stability, ver 2.5, November 2019.

- Eyre, J. R., English, S. J., and Forsythe, M.: Assimilation of satellite data in numerical weather prediction. Part I: The early years, *Quarterly Journal of the Royal Meteorological Society*, 146, 49–68, <https://doi.org/10.1002/qj.3654>, 2020.
- 840 Fox, S., Lee, C., Moyna, B., Philipp, M., Rule, I., Rogers, S., King, R., Oldfield, M., Rea, S., Henry, M., Wang, H., and Harlow, R. C.: ISMAR: an airborne submillimetre radiometer, *Atmospheric Measurement Techniques*, 10, 477–490, <https://doi.org/10.5194/amt-10-477-2017>, 2017.
- Fox, S., A. Vance, E. Turner, D. Cimini, D. Gallucci, F. Romano, C. Prigent, J. Pardo: ISMAR study final report, EUMETSAT study report, 2023.
- 845 Gallucci D., D. Cimini, E. Turner, S. Fox, P. Rosenkranz, M. Tretyakov, V. Mattioli, S. Larosa, and F. Romano: Uncertainty of simulated brightness temperature due to sensitivity to atmospheric gas spectroscopic parameters, (to be submitted to ACP), 2023
- Geer, A. J., Bauer, P., Lonitz, K., Barlakas, V., Eriksson, P., Mendrok, J., Doherty, A., Hocking, J., and Chambon, P.: Bulk hydrometeor optical properties for microwave and sub-millimetre radiative transfer in RTTOV-SCATT v13.0, *Geosci. Model Dev.*, 14, 7497–7526, <https://doi.org/10.5194/gmd-14-7497-2021>, 2021.
- 850 Gordon, I. E., Rothman, L. S., Hill, C., Kochanov, R. V., Tan, Y., Bernath, P. F., Birk, M., Boudon, V., Campargue, A., Chance, K. V., Drouin, B. J., Flaud, J.-M., Gamache, R. R., Hodges, J. T., Jacquemart, D., Perevalov, V. I., Perrin, A., Shine, K. P., Smith, M.-A. H., Tennyson, J., Toon, G. C., Tran, H., Tyuterev, V. G., Barbe, A., Császár, A. G., Devi, V. M., Furtenbacher, T., Harrison, J. J., Hartmann, J.-M., Jolly, A., Johnson, T. J., Karman, T., Kleiner, I., Kyuberis, A. A., Loos, J., Lyulin, O. M., Massie, S. T., Mikhailenko, S. N., Moazzen-Ahmadi, N., Müller, H. S. P., Naumenko, O. V., Nikitin, A. V., Polyansky, O. L., Rey, M., Rotger, M., Sharpe, S. W., Sung, K., Starikova, E., Tashkun, S. A., Auwera, J. V., Wagner, G., Wilzewski, J., Wcisło, P., Yu, S., and Zak, E. J.: The HITRAN2016 molecular spectroscopic database, *Journal of Quantitative Spectroscopy and Radiative Transfer*, 203, 3–69, <https://doi.org/10.1016/j.jqsrt.2017.06.038>, 2017.
- 860 Han, Y., van Delst, P., Liu, Q., Weng, F., Yan, B., Treadon, R., and Derber, J.: JCSDA Community Radiative Transfer Model (CRTM) : version 1, 2006.
- Hersbach, H., Bell, B., Berrisford, P., Hirahara, S., Horányi, A., Muñoz-Sabater, J., Nicolas, J., Peubey, C., Radu, R., Schepers, D., Simmons, A., Soci, C., Abdalla, S., Abellan, X., Balsamo, G., Bechtold, P., Biavati, G., Bidlot, J., Bonavita, M., De Chiara, G., Dahlgren, P., Dee, D., Diamantakis, M., Dragani, R., Flemming, J., Forbes, R., 865 Fuentes, M., Geer, A., Haimberger, L., Healy, S., Hogan, R. J., Hólm, E., Janisková, M., Keeley, S., Laloyaux, P., Lopez, P., Lupu, C., Radnoti, G., de Rosnay, P., Rozum, I., Vamborg, F., Villaume, S., and Thépaut, J.-N.: The ERA5 global reanalysis, *Quarterly Journal of the Royal Meteorological Society*, 146, 1999–2049, <https://doi.org/10.1002/qj.3803>, 2020.

- 870 Hocking, J., Vidot, J., Brunel, P., Roquet, P., Silveira, B., Turner, E., and Lupu, C.: A new gas absorption optical depth parameterisation for RTTOV version 13, *Geoscientific Model Development*, 14, 2899–2915, <https://doi.org/10.5194/gmd-14-2899-2021>, 2021.
- Hogan, R. J., Honeyager, R., Tyynelä, J., and Kneifel, S.: Calculating the Millimetre-Wave Scattering Phase Function of Snowflakes Using the Self-Similar Rayleigh–Gans Approximation, *Q. J. Roy. Meteor. Soc.*, 143, 834–844, <https://doi.org/10.1002/qj.2968>, 2017.
- 875 Holdridge, D.: Balloon-Borne Sounding System (SONDE) Instrument Handbook, Atmospheric Radiation Measurement user facility, Pacific Northwest National Laboratory, Richland, WA, <https://doi.org/10.2172/1020712>, 2020.
- ITU-R Recommendation P.835-6, Reference standard atmospheres, available at <https://www.itu.int/rec/R-REC-P.835/en>, Last accessed: 26 July 2021, approved December 2017.
- 880 Karpowicz, B. M., Stegmann, P. G., Johnson, B. T., Christophersen, H. W., Hyer, E. J., Lambert, A., and Simon, E.: pyCRTM: A python interface for the community radiative transfer model, *Journal of Quantitative Spectroscopy and Radiative Transfer*, 288, 108263, <https://doi.org/10.1016/j.jqsrt.2022.108263>, 2022.
- Keeler, E. and Burk, K.: Balloon-Borne Sounding System (SONDEWNP), <https://doi.org/10.5439/1595321>, 2012.
- 885 Koshelev, M. A., Golubiatnikov, G. Yu., Vilkov, I. N., and Tretyakov, M. Yu.: Line shape parameters of the 22-GHz water line for accurate modeling in atmospheric applications, *Journal of Quantitative Spectroscopy and Radiative Transfer*, 205, 51–58, <https://doi.org/10.1016/j.jqsrt.2017.09.032>, 2018.
- Koshelev, M. A., Vilkov, I. N., Makarov, D. S., Tretyakov, M. Yu., Vispoel, B., Gamache, R. R., Cimini, D., Romano, F., and Rosenkranz, P. W.: Water vapor line profile at 183-GHz: Temperature dependence of broadening, shifting, and speed-dependent shape parameters, *Journal of Quantitative Spectroscopy and Radiative Transfer*, 262, 107472, <https://doi.org/10.1016/j.jqsrt.2020.107472>, 2021.
- 890 Koshelev, M. A., Golubiatnikov, G. Yu., Vilkov, I. N., and Tretyakov, M. Yu.: Molecular oxygen fine structure with sub-kHz accuracy, *Journal of Quantitative Spectroscopy and Radiative Transfer*, 278, 108001, <https://doi.org/10.1016/j.jqsrt.2021.108001>, 2022.
- 895 Larosa, S., Cimini, D., Gallucci, D., Di Paola, F., Nilo, S. T., Ricciardelli, E., Ripepi, E., and Romano, F.: A Cloud Detection Neural Network Approach for the Next Generation Microwave Sounder Aboard EPS MetOp-SG A1, *Remote Sensing*, 15, 1798, <https://doi.org/10.3390/rs15071798>, 2023.
- Liebe, H. J.: MPM—An atmospheric millimeter-wave propagation model, *Int J Infrared Milli Waves*, 10, 631–650, <https://doi.org/10.1007/BF01009565>, 1989.

- 900 Liebe, H. J., Hufford, G. A., and Manabe, T.: A model for the complex permittivity of water at frequencies below 1 THz, *Int J Infrared Milli Waves*, 12, 659–675, <https://doi.org/10.1007/BF01008897>, 1991.
- Liebe, H. J., Hufford, G. A., and Cotton, M.: Propagation modeling of moist air and suspended water/ice particles at frequencies below 1000 GHz, In *AGARD*, 1993.
- 905 Liljegren, J. C., Boukabara, S.-A., Cady-Pereira, K., and Clough, S. A.: The effect of the half-width of the 22-GHz water vapor line on retrievals of temperature and water vapor profiles with a 12-channel microwave radiometer, *IEEE Transactions on Geoscience and Remote Sensing*, 43, 1102–1108, <https://doi.org/10.1109/TGRS.2004.839593>, 2005.
- Löhnert, U. and Maier, O.: Operational profiling of temperature using ground-based microwave radiometry at Payerne: prospects and challenges, *Atmospheric Measurement Techniques*, 5, 1121–1134, <https://doi.org/10.5194/amt-5-1121-2012>, 2012.
- 910 Makarov, D. S., Tretyakov, M. Yu., and Rosenkranz, P. W.: Revision of the 60-GHz atmospheric oxygen absorption band models for practical use, *Journal of Quantitative Spectroscopy and Radiative Transfer*, 243, 106798, <https://doi.org/10.1016/j.jqsrt.2019.106798>, 2020.
- Martinet, P., Cimini, D., De Angelis, F., Canut, G., Unger, V., Guillot, R., Tzanos, D., and Paci, A.: Combining ground-based microwave radiometer and the AROME convective scale model through 1DVAR retrievals in complex terrain: an Alpine valley case study, *Atmospheric Measurement Techniques*, 10, 3385–3402, <https://doi.org/10.5194/amt-10-3385-2017>, 2017.
- 915 Martinet, P., Cimini, D., Burnet, F., Ménétrier, B., Michel, Y., and Unger, V.: Improvement of numerical weather prediction model analysis during fog conditions through the assimilation of ground-based microwave radiometer observations: a 1D-Var study, *Atmospheric Measurement Techniques*, 13, 6593–6611, <https://doi.org/10.5194/amt-13-6593-2020>, 2020.
- 920 Marzano, F. S., Mugnai, A., Panegrossi, G., Pierdicca, N., Smith, E. A., and Turk, J.: Bayesian estimation of precipitating cloud parameters from combined measurements of spaceborne microwave radiometer and radar, *IEEE Transactions on Geoscience and Remote Sensing*, 37, 596–613, <https://doi.org/10.1109/36.739124>, 1999.
- 925 Matricardi, M.: The generation of RTTOV regression coefficients for IASI and AIRS using a new profile training set and a new line-by-line database, *ECMWF Technical Memoranda*, 47, <https://doi.org/10.21957/59u3oc9es>, 2008.
- 930 Mech, M., Maahn, M., Kneifel, S., Ori, D., Orlandi, E., Kollias, P., Schemann, V., and Crewell, S.: PAMTRA 1.0: the Passive and Active Microwave radiative TRANSfer tool for simulating radiometer and radar measurements of the cloudy atmosphere, *Geoscientific Model Development*, 13, 4229–4251, <https://doi.org/10.5194/gmd-13-4229-2020>, 2020.

- 935 Mlawer, E. J., Payne, V. H., Moncet, J.-L., Delamere, J. S., Alvarado, M. J., and Tobin, D. C.: Development and recent evaluation of the MT_CKD model of continuum absorption, *Philosophical Transactions of the Royal Society A: Mathematical, Physical and Engineering Sciences*, 370, 2520–2556, <https://doi.org/10.1098/rsta.2011.0295>, 2012.
- Mollière, P., Wardenier, J. P., Boekel, R. van, Henning, T., Molaverdikhani, K., and Snellen, I. a. G.: petitRADTRANS - A Python radiative transfer package for exoplanet characterization and retrieval, *A&A*, 627, A67, <https://doi.org/10.1051/0004-6361/201935470>, 2019.
- 940 Moradi, I., Ferraro, R. R., Eriksson, P., and Weng, F.: Intercalibration and Validation of Observations From ATMS and SAPHIR Microwave Sounders, *IEEE Transactions on Geoscience and Remote Sensing*, 53, 5915–5925, <https://doi.org/10.1109/TGRS.2015.2427165>, 2015.
- Payne, V. H., Delamere, J. S., Cady-Pereira, K. E., Gamache, R. R., Moncet, J.-L., Mlawer, E. J., and Clough, S. A.: Air-Broadened Half-Widths of the 22- and 183-GHz Water-Vapor Lines, *IEEE Transactions on Geoscience and Remote Sensing*, 46, 3601–3617, <https://doi.org/10.1109/TGRS.2008.2002435>, 2008.
- 945 Petty, G. W.: *A First Course in Atmospheric Radiation*, Sundog Pub., 2006.
- Picard, G., Brucker, L., Fily, M., Gallée, H., and Krinner, G.: Modeling time series of microwave brightness temperature in Antarctica, *Journal of Glaciology*, 55, 537–551, <https://doi.org/10.3189/002214309788816678>, 2009.
- 950 Picard, G., Sandells, M., and Löwe, H.: SMRT: an active–passive microwave radiative transfer model for snow with multiple microstructure and scattering formulations (v1.0), *Geoscientific Model Development*, 11, 2763–2788, <https://doi.org/10.5194/gmd-11-2763-2018>, 2018.
- Rosenkranz, P.: *Absorption of Microwaves by Atmospheric Gases*, John Wiley and Sons, 1993.
- Rosenkranz, P.: Line-by-line microwave radiative transfer (non-scattering), , <https://doi.org/10.21982/M81013>, 2017.
- 955 Rosenkranz, P. W.: Interference coefficients for overlapping oxygen lines in air, *Journal of Quantitative Spectroscopy and Radiative Transfer*, 39, 287–297, [https://doi.org/10.1016/0022-4073\(88\)90004-0](https://doi.org/10.1016/0022-4073(88)90004-0), 1988.
- Rosenkranz, P. W.: Water vapor microwave continuum absorption: A comparison of measurements and models, *Radio Science*, 33, 919–928, <https://doi.org/10.1029/98RS01182>, 1998.
- 960 Rosenkranz, P. W.: Retrieval of temperature and moisture profiles from AMSU-A and AMSU-B measurements, *IEEE Transactions on Geoscience and Remote Sensing*, 39, 2429–2435, <https://doi.org/10.1109/36.964979>, 2001.
- Rosenkranz, P. W.: Comment on “Uncertainties in the temperature dependence of the line-coupling parameters of the microwave oxygen band: impact study,” *IEEE Transactions on Geoscience and Remote Sensing*, 43, 2160–2161, <https://doi.org/10.1109/TGRS.2005.853189>, 2005.

- 965 Rosenkranz, P. W.: A Model for the Complex Dielectric Constant of Supercooled Liquid Water at Microwave Frequencies, *IEEE Transactions on Geoscience and Remote Sensing*, 53, 1387–1393, <https://doi.org/10.1109/TGRS.2014.2339015>, 2015.
- 970 Rosenkranz, P. W., Cimini, D., Koshelev, M. A., and Tretyakov, M. Yu.: Covariances of Spectroscopic Parameter Uncertainties in Microwave Forward Models and Consequences for Remote Sensing, in: 2018 IEEE 15th Specialist Meeting on Microwave Radiometry and Remote Sensing of the Environment (MicroRad), 2018 IEEE 15th Specialist Meeting on Microwave Radiometry and Remote Sensing of the Environment (MicroRad), 1–6, <https://doi.org/10.1109/MICRORAD.2018.8430729>, 2018.
- Rosenkranz, P. W. and Cimini, D.: Speed Dependence of 22- and 118-GHz Line Shapes for Tropospheric Remote Sensing, *IEEE Transactions on Geoscience and Remote Sensing*, 57, 9702–9708, <https://doi.org/10.1109/TGRS.2019.2928570>, 2019.
- 975 Rothman, L. S., Jacquemart, D., Barbe, A., Chris Benner, D., Birk, M., Brown, L. R., Carleer, M. R., Chackerian, C., Chance, K., Coudert, L. H., Dana, V., Devi, V. M., Flaud, J.-M., Gamache, R. R., Goldman, A., Hartmann, J.-M., Jucks, K. W., Maki, A. G., Mandin, J.-Y., Massie, S. T., Orphal, J., Perrin, A., Rinsland, C. P., Smith, M. A. H., Tennyson, J., Tolchenov, R. N., Toth, R. A., Vander Auwera, J., Varanasi, P., and Wagner, G.: The HITRAN 2004 molecular spectroscopic database, *Journal of Quantitative Spectroscopy and Radiative Transfer*, 96, 139–204, <https://doi.org/10.1016/j.jqsrt.2004.10.008>, 2005.
- 980 Rufenacht, R., Haeefe, A., Pospichal, B., Cimini, D., Bircher-Adrot, S., Turp, M., and Sugier, J.: EUMETNET opens to microwave radiometers for operational thermodynamical profiling in Europe, *Bull. of Atmos. Sci. & Technol.*, 2, 4, <https://doi.org/10.1007/s42865-021-00033-w>, 2021.
- 985 Sanò, P., Panegrossi, G., Casella, D., Di Paola, F., Milani, L., Mugnai, A., Petracca, M., and Dietrich, S.: The Passive microwave Neural network Precipitation Retrieval (PNPR) algorithm for AMSU/MHS observations: description and application to European case studies, *Atmospheric Measurement Techniques*, 8, 837–857, <https://doi.org/10.5194/amt-8-837-2015>, 2015.
- 990 Saunders, R., Hocking, J., Turner, E., Rayer, P., Rundle, D., Brunel, P., Vidot, J., Roquet, P., Matricardi, M., Geer, A., Bormann, N., and Lupu, C.: An update on the RTTOV fast radiative transfer model (currently at version 12), *Geoscientific Model Development*, 11, 2717–2737, <https://doi.org/10.5194/gmd-11-2717-2018>, 2018.
- Schreier, F., Gimeno García, S., Hedelt, P., Hess, M., Mendrok, J., Vasquez, M., and Xu, J.: GARLIC — A general purpose atmospheric radiative transfer line-by-line infrared-microwave code: Implementation and evaluation, *Journal of Quantitative Spectroscopy and Radiative Transfer*, 137, 29–50, <https://doi.org/10.1016/j.jqsrt.2013.11.018>, 2014.
- 995 Schreier, F., Computational aspects of speed-dependent Voigt profiles, *Journal of Quantitative Spectroscopy and Radiative Transfer*, 187, 44–53, <https://doi.org/10.1016/j.jqsrt.2016.08.009>, 2017.

Schreier, F., Gimeno García, S., Hochstaffl, P., and Städt, S.: Py4CA_TS—PYthon for Computational ATmospheric Spectroscopy, *Atmosphere*, 10, 262, <https://doi.org/10.3390/atmos10050262>, 2019.

Schreier, F., Hochstaffl, P., Computational aspects of speed-dependent Voigt and Rautian profiles, *Journal of Quantitative Spectroscopy and Radiative Transfer*, 258, 107385, <https://doi.org/10.1016/j.jqsrt.2020.107385>, 2021.

Schroeder, J. A. and Westwater, E. R.: Users' guide to WPL microwave radiative transfer software, 1991.

Shrestha, B., Brotzge, J. A., and Wang, J.: Evaluation of the New York State Mesonet Profiler Network data, *Atmospheric Measurement Techniques*, 15, 6011–6033, <https://doi.org/10.5194/amt-15-6011-2022>, 2022.

Titos, G., Jefferson, A., Sheridan, P. J., Andrews, E., Lyamani, H., Alados-Arboledas, L., and Ogren, J. A.: Aerosol light-scattering enhancement due to water uptake during the TCAP campaign, *Atmospheric Chemistry and Physics*, 14, 7031–7043, <https://doi.org/10.5194/acp-14-7031-2014>, 2014.

Tretyakov, M. Y., Parshin, V. V., Koshelev, M. A., Shanin, V. N., Myasnikova, S. E., and Krupnov, A. F.: Studies of 183GHz water line: broadening and shifting by air, N₂ and O₂ and integral intensity measurements, *Journal of Molecular Spectroscopy*, 218, 239–245, [https://doi.org/10.1016/S0022-2852\(02\)00084-X](https://doi.org/10.1016/S0022-2852(02)00084-X), 2003.

Tretyakov, M. Yu.: Spectroscopy underlying microwave remote sensing of atmospheric water vapor, *Journal of Molecular Spectroscopy*, 328, 7–26, <https://doi.org/10.1016/j.jms.2016.06.006>, 2016.

Tretyakov, M. Yu., Koshelev, M. A., Dorovskikh, V. V., Makarov, D. S., and Rosenkranz, P. W.: 60-GHz oxygen band: precise broadening and central frequencies of fine-structure lines, absolute absorption profile at atmospheric pressure, and revision of mixing coefficients, *Journal of Molecular Spectroscopy*, 231, 1–14, <https://doi.org/10.1016/j.jms.2004.11.011>, 2005.

Tripoli, G. J., Medaglia, C. M., Dietrich, S., Mugnai, A., Panegrossi, G., Pinori, S., and Smith, E. A.: The 9–10 November 2001 Algerian Flood: A Numerical Study, *Bulletin of the American Meteorological Society*, 86, 1229–1235, 2005.

Tritsis, A., Yorke, H., and Tassis, K.: Python Radiative Transfer Emission code (pyrate): non-local thermodynamic equilibrium spectral lines simulations, *Monthly Notices of the Royal Astronomical Society*, 478, 2056–2064, <https://doi.org/10.1093/mnras/sty1152>, 2018.

Turner, D. D. and Löhnert, U.: Ground-based temperature and humidity profiling: combining active and passive remote sensors, *Atmospheric Measurement Techniques*, 14, 3033–3048, <https://doi.org/10.5194/amt-14-3033-2021>, 2021.

Turner, D. D., Cadeddu, M. P., Lohnert, U., Crewell, S., and Vogelmann, A. M.: Modifications to the Water Vapor Continuum in the Microwave Suggested by Ground-Based 150-GHz Observations, *IEEE Transactions on Geoscience and Remote Sensing*, 47, 3326–3337, <https://doi.org/10.1109/TGRS.2009.2022262>, 2009.

- 1030 Turner, E., Rayer, P., and Saunders, R.: AMSUTRAN: A microwave transmittance code for satellite remote sensing, *Journal of Quantitative Spectroscopy and Radiative Transfer*, 227, 117–129, <https://doi.org/10.1016/j.jqsrt.2019.02.013>, 2019.
- Vermote, E. F., Tanre, D., Deuze, J. L., Herman, M., and Morcette, J.-J.: Second Simulation of the Satellite Signal in the Solar Spectrum, 6S: an overview, *IEEE Transactions on Geoscience and Remote Sensing*, 35, 675–686, <https://doi.org/10.1109/36.581987>, 1997.
- 1035 Wang, D., Prigent, C., Kilic, L., Fox, S., Harlow, C., Jimenez, C., Aires, F., Grassotti, C., and Karbou, F.: Surface Emissivity at Microwaves to Millimeter Waves over Polar Regions: Parameterization and Evaluation with Aircraft Experiments, *Journal of Atmospheric and Oceanic Technology*, 34, 1039–1059, <https://doi.org/10.1175/JTECH-D-16-0188.1>, 2017.
- 1040 Wei, S.-W., Lu, C.-H. (Sarah), Johnson, B. T., Dang, C., Stegmann, P., Grogan, D., Ge, G., and Hu, M.: The Influence of Aerosols on Satellite Infrared Radiance Simulations and Jacobians: Numerical Experiments of CRTM and GSI, *Remote Sensing*, 14, 683, <https://doi.org/10.3390/rs14030683>, 2022.
- Wilson, R. T.: Py6S: A Python interface to the 6S radiative transfer model, *Computers & Geosciences*, 51, 166–171, <https://doi.org/10.1016/j.cageo.2012.08.002>, 2013.